Alma Mater Studiorum - Università di Bologna

SCUOLA DI SCIENZE

Dipartimento di Chimica Industriale “Toso Montanari”

Corso di Laurea Magistrale in

Chimica Industriale

Curriculum: Advanced Spectroscopy in Chemistry

Classe LM-71 - Scienze e Tecnologie della Chimica Industriale

Damping and Thermomechanical behaviour of CFRP laminates modified with rubbery nanofibers

Candidate

Jonas Nehr

Supervisor

Prof. Laura Mazzocchetti

Co-Supervisor

Emanuelle Maccaferri

Academic Year 2019-2020

Abstract

Nanofibrous membranes are a promising material for tailoring the properties of laminated CFRP composites by embedding them into the structure. This project aimed to understand the effect of number, position and thickness of nanofibrous modifications specifically on the damping behaviour of the resulting nano-modified CFRP composite with an epoxy matrix. An improvement of damping capacity is expected to improve a composites lifetime and fatigue resistance by prohibiting the formation of microcracks and consequently hindering delamination, it also promises a rise in comfort for a range of final products by intermission of vibration propagation and therefore diminution of noise. Electrospinning was the technique employed to produce nanofibrous membranes from a blend of polymeric solutions. SEM, WAXS and DSC were utilised to evaluate the quality of the obtained membranes before they were introduced, following a specific stacking sequence, in the production process of the laminate. A suitable curing cycle in an autoclave was applied to mend the modifications together with the matrix material, ensuring full crosslinking of the matrix and therefore finalising the production process. DMA was exercised in order to gain an understanding about the effects of the different modifications on the properties of the composite. During this investigation it became apparent that a high number of modifications of laminate CFRP composites, with an epoxy matrix, with thick rubbery nanofibrous membranes has a positive effect on the damping capacity and the temperature range the effect applies in. A suggestion for subsequent studies as well as a recommendation for the production of nano-modified CFRP structures is included at the end of this document.

Table of contents

Common Abbreviations

CFRP	Carbon fibre reinforced polymer
Cm	centimetre
DMA	Dynamic mechanical analysis
E	Elastic Modulus
E´	Conservative Modulus
E´´	Dissipative Modulus
FRP	Fibre reinforced polymers
FWHM	Full Width at Half Maximum
GPa	giga Pascal
h	hour
Hz	Hertz
J	Joule
kV	kilo Volt
kN	kilo Newton
mA	milli Ampere
min	minutes
Mw	molecular weight
MPa	mega Pascal
NBR	nitrile butadiene rubber
nm	nanometre
PAN	Polyacrylonitrile
PCL	Poly-(ε-caprolactone)
rpm	revolutions per minute
RTM	Resin Transfer Moulding
SEM	Scanning electron microscopy

T_g	Glass transition temperature
T_m	Melting temperature
µm	micrometre
°C	degree Celsius
%mol	molar percentage
%wt	weight percentage

1 Introduction

1.1 Composite materials

The construction of a variety of products ranging from large scale like buildings, ships, airplanes over cars, household devices to medical applications or computer sciences benefits from the use of composite materials today.

The term composite material describes a material that is built out of a combination of several heterogenous components. A product obtained by the union of these, so called phases, will possess properties that neither one of the starting materials show[1].

Usually composite materials are made up from matrix and reinforcement. The matrix being the continuous phase has the purpose to hold the shape of the compound and distributes loads onto the reinforcement. It also protects the reinforcement from mechanical damage and the chemical environment. Matrices can be made up from a number of materials like ceramics, metals and polymers. The reinforcement can be particle shaped or fibrous and bears the task of supporting most of the mechanical stress the compound is subjected to and therefore is responsible for the mechanical strength of the composite. In order to be characterised as such the reinforcement must have a considerably higher rigidity, i.e. high Elastic Modulus (E), than the matrix. If the difference, in rigidity, between matrix and the incorporated material is negligible it can be considered as a filler rather than a reinforcement. While matrix and reinforcement are chosen to adjust the structural, mechanical or chemical properties of the compound, fillers can be varied in order to adjust parameters such as colour, weight, surface texture or electrical and thermal conductivity[2,3].

The production of a composite is therefore successful if the chosen components have a high ability to couple together without changing their respective properties. In such a case a material can be produced, that has tailorable characteristics varying far from those of traditional materials such as ceramics, steel, aluminium, iron, common polymers or wood. Combinations of materials can be chosen for the relevant properties, ease of fabrication, availability, relative cost, etc.[4]. To illustrate: reinforced concrete exploits the high tensile and flexural strength of steel in order to overcome the lack of it in concrete[5]. Composites reinforced with carbon fibres can show a similar elastic

modulus to that of steel while maintaining a far lower density. Following these examples composite materials introduce a superior quality in a variety of applications opening up new fields of construction or improvements of already accustomed products.

Due to the aim of this project and to specify, I will elaborate on the properties, advantages and disadvantages of carbon fibre reinforced polymers (CFRPs) in the following.

1.2 Carbon fibre reinforced polymer

In the production of high-performance composites, the most commonly used matrices are either thermosetting polymers. In comparison to those, thermoplastic materials can be repeatably fluidified by heating over their intrinsic glass transition temperature (T_g) or melting temperature (T_m) which enables them to be easily reshaped and also recycled. Thermosetting materials, so called resins, as opposed to the aforementioned are usually viscous liquids at room temperature and become irreversibly solid when they go through a curing cycle. These resins, which are usually made up from phenolic or epoxy polymers, form covalent bonds between their polymeric chains. As this so-called crosslinking, happens slowly at room temperature, the process can be sped up and controlled during the curing cycle by applying pressure and heat to the specimen.

Thermoplastic polymers can be amorphous or semicrystalline, the latter is characterised by the possession of both a T_g and T_m while an amorphous thermoplastic, similar to a thermoset polymer only exhibits a T_g. This allows semicrystalline thermoplastic polymers to be reshaped in the temperature frame between their T_g and T_m while both amorphous thermoplastics and thermoset polymers start to deteriorate above their T_g, prohibiting any reshaping or direct recycling for the latter.

Next to the discussed thermal stability the excellent adhesive properties towards fibrous reinforcements, a good chemical resistance and high mechanical properties are reasons for thermosets to be more and more used every day.

The most common use is in combination with fibrous reinforcements. These fibre reinforced polymers (FRP) are made up from a thermoset resin and are classified due to the length and diameter of the used fibres. While the mechanical properties of the fibres, and therefore of the composite, depend on the fibrous diameter, the adhesion to the matrix increases with a declining diameter, due to a higher surface-to-volume ratio[6]. In order to achieve a significant reinforcement in the composite not only the strength

of this interfacial fibre-matrix bond is important but also the fibres length. Since the fibres cannot contribute to the strength and stiffness of a structure at their end the alleged load condition implies a certain critical length which the fibres must exceed in order to exhibit an effect throughout the whole structure and to be called continuous fibres[7]. Another aspect resulting from the type of fibres lies in their orientation. While randomly oriented fibres allow the material equal structural properties into all directions a determined orientation creates tuneable properties for different spatial direction. To illustrate on an extreme case: Composites with continuous aligned fibres carry a tensile load in the fibres direction in full isotropy, but while loading them perpendicular to the fibres orientation the structure has similar properties to the matrix and therefore show no reinforcement effect[8]. In consequence long fibre composites inherit superior mechanical properties compared to conventional polymeric materials[9].

A common example for a composite of long fibres and resins are carbon fibre reinforced polymers (CFRPs). They were first introduced in aeronautics for that they exhibit high mechanical performance (i.e. high corrosion resistance, high elastic modulus and tensile strength) while maintaining exceptional low weight. In addition to the advantages of a low density and unique production methods, the reciprocal increase in numbers of applications and a decrease in production cost allows the material to enjoy a growing market sector while replacing more and more conventional materials[8,10].

Table 1: Estimated global consumption of carbon fibres[11].

	1999 (tons)	2004 (tons)	2006 (tons)	2008 (tons)	2010 (tons)
Aerospace	4,000	5,600	6,500	7,500	9,800
Industrial	8,100	11,400	12,800	15,600	17,500
Sporting Goods	4,500	4,900	5,900	6,700	6,900
Total	16,600	21,900	25,200	29,800	34,200

While Table 1 shows the global carbon fibre consumption, a number of at this point in time employed applications of these materials are listed in Figure 1 below.

Figure 1: Examples of CFRP applications[12–15].

1.2.1 Production of Carbon fibres

Carbon fibres were first produced in 1878 by Edison, who used them in incandescent lamps, but only underwent commercial production due to a process formulated by William Watt in 1960 who already aimed to use them for their high tensile strength and elastic modulus[16,17]. He introduced the thermal degradation of organic materials until complete carbonisation. Even today the production of carbon fibres is done by performing the controlled pyrolysis of carbon-containing precursors like polyacrylonitrile (PAN) [18]. PAN is with 90% of production the most common precursor for carbon fibre production today[19]. The production process involves the following steps: first an acrylonitrile powder is mixed with another plastic, for example methyl acrylate, and will then undergo a catalysed suspension or solution polymerisation process.

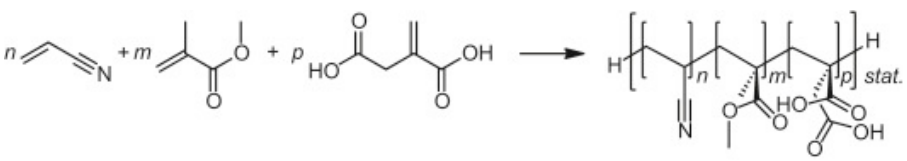

Figure 2: Synthesis of a typical terpolymer consisting of acrylonitrile, methyl methacrylate, and itaconic acid[20].

The obtained polyacrylonitrile plastic, shown in Figure 2, is then jet spun into fibres by a solvent evaporation step into a chemical bath or quenching chamber, as pictured in the following Figure 3.

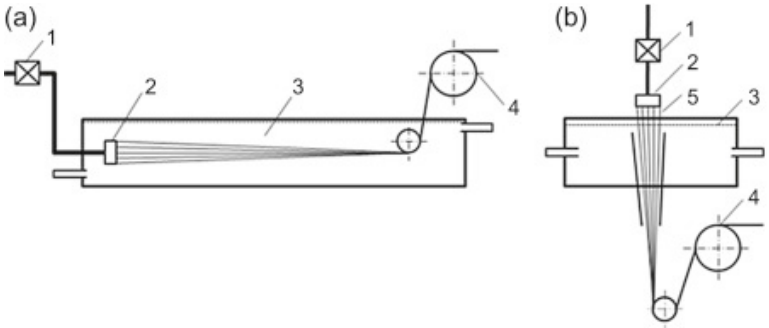

Figure 3: Schemes of (a) wet and (b) dry jet spinning techniques. 1, metering pump; 2, spinneret; 3, coagulation bath; 4, take-up godet; 5, air gap[20].

Although the fibres obtain their internal atomic structure during the spinning process their size allows the fibres to be washed and stretched to the desired diameter. Before the fibres undergo full carbonisation, they will be stabilised during a heating step to 200-300°C for 30-120 min in air. This oxidation yields a cyclisation, however the complexity and high dependence of environmental adjustment parameters, namely temperature and chemical environment leads to an open discussion about the reaction mechanism. The following Figure 4 shows some of the currently proposed reaction steps.

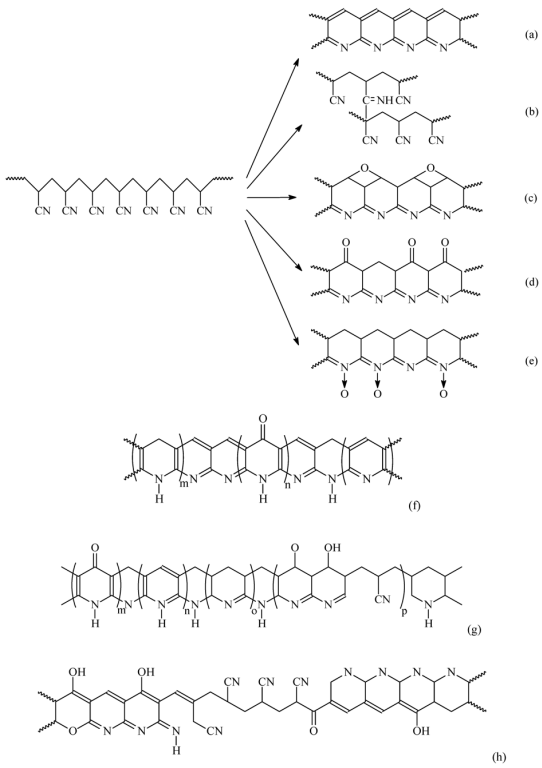

Figure 4: PAN Stabilisation[11].

Since the stabilisation is an exotherm process the temperature has to be carefully controlled throughout the process to maintain a homogenous result[21].

Before a second heating step towards 1000-3000°C, lasting several minutes, in an oxygen deprived atmosphere to evaporate the non-carbon atoms, like water or ammonia, which leads the remaining carbon crystals to a tightly packed structure aligned to the longitudinal axis of the fibre[19].

Table 2: Comparison of the mechanical properties of carbon fibres to other materials[22].

Material	Density (ρ)	Tensile Strength	Specific Tensile Strength	Young´s modulus (E)	Specific Modulus
Unit	g/cm^3	MPa	kN*m/kg	GPa	E/ρ
Steel	7,8	365	46,4	200,0	25,6
Titanium	4,5	344	76,0	116,0	25,8
Aluminium	2,8	572	204,0	69,0	24,6
Glass Fibre	2,5	3400	1307,0	81,0	32,4
Kevlar Fibre	1,4	3620	2514,0	70,5	50,4
Carbon Fibre	1,9	4300	2457,0	181,0	95,3

As exhibited in Table 2 the Young´s modulus, that is a measure of a materials stiffness, of these carbon fibres is comparable to that of steel and significantly higher compared to other fibres such as glass or Kevlar. Considering the tensile strength carbon fibres are in the realm of Kevlar and therefore superior to steel. At last the biggest advantage of carbon fibres is their low density, about a quarter of steel and half of glass fibres[23]. The effect can be seen while comparing the specific moduli in Table 2. The specific modulus shows how far the carbon fibres stiffness to weight ratio exceed the values of the competitors. This advantage creates the already mentioned ability to build products with comparable or even superior mechanical properties while also cutting the weight by a big margin[24].

1.2.2 Production of CFRP

For the purpose of manufacturing carbon fibres can be considered equivalent to usual yarns, like cotton or wool and can therefore be processed accordingly with the appropriate equipment. As a result, different weave patterns can be produced. Some examples are shown in the following Figure 5 and even mats produced of randomly oriented fibres can be used for further production steps.

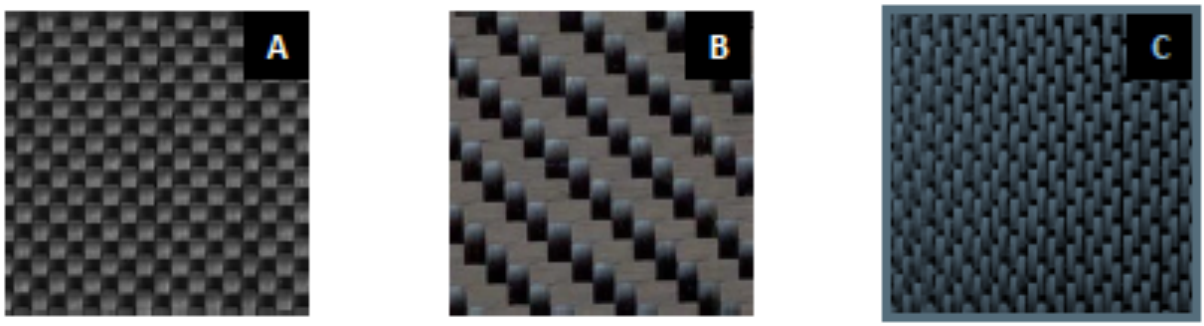

Figure 5: (A) plain weave; (B) Twill weave; (C) Satin weave [24]

The actual production of CFRP materials can be done manually which is a simple and versatile technique that is best used to form highly individual, detailed or complex shapes. In this way the weaved fabric is placed in a mould, resembling the desired structure, and the liquid resin is casted into the mould and spread with a roller. This laborious process is repeated with multiple layers of fabric until the desired shape and thickness is obtained and the cast, aided by the mould, is sealed and put in an auto-clave for the following curing step[24]. While applying vacuum, pressure and heat to the specimen possible air bubbles will be extracted and the resin will be cured changing the sample into the aimed solid structure. In order to aid understanding the following Figure 6 is included[25].

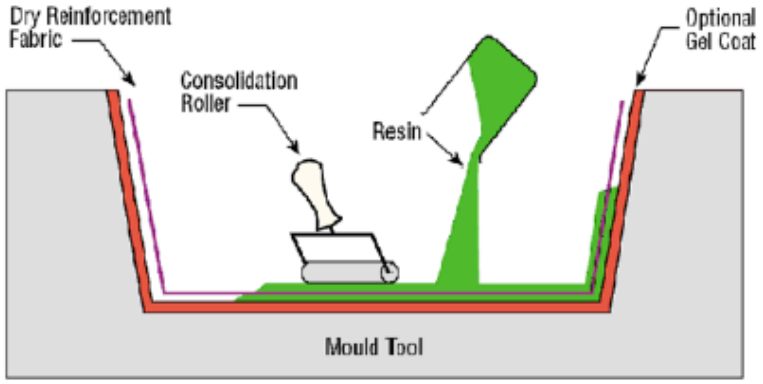

Figure 6: Schematic explanation of manual mould casting of CFRP materials[24].

Resin Transfer Moulding (RTM) is a useful variant to consider ensuring a reduction in labour cost. In this process the fabric is as well placed in a mould but sealed with a sheet of plastic material and the resin impregnation is carried out by pressurised injec-tion into the cavity. This can also be done while the mould is already held under vac-uum to help with the impregnation. Figure 7 demonstrates the principle of the process.

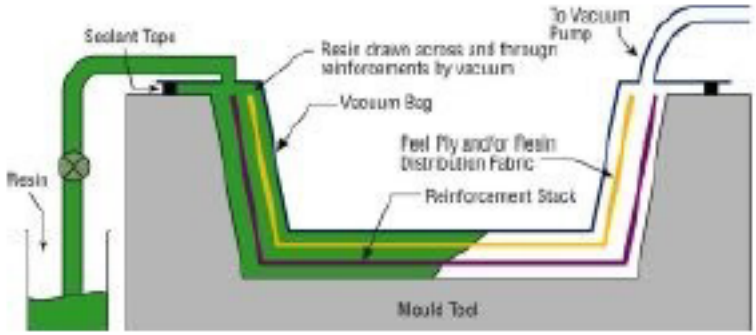

Figure 7: Schematic representation of Resin Transfer Moulding (RTM)[24].

The advantages of this technique are the increased uniformity in impregnation and the degree to which the process can be automatised.

In general crosslinking can be done at room temperature or while heating, depending on the properties of the used resin, the timeframe for the production of the composite and the planned application of the latter. However, a limitation is the fact that irregular prohibit full resin impregnation in the corners of an irregular structure.

Another technique which is often employed for CFRP production is the use of pre-impregnated fabrics with partially crosslinked resin. Due to stacking these, so called prepregs, until the desired shape and thickness is reached and leading them through the appropriate curing cycle finally forming macroscopically a single structural element which is therefore considered a laminated CFRP.

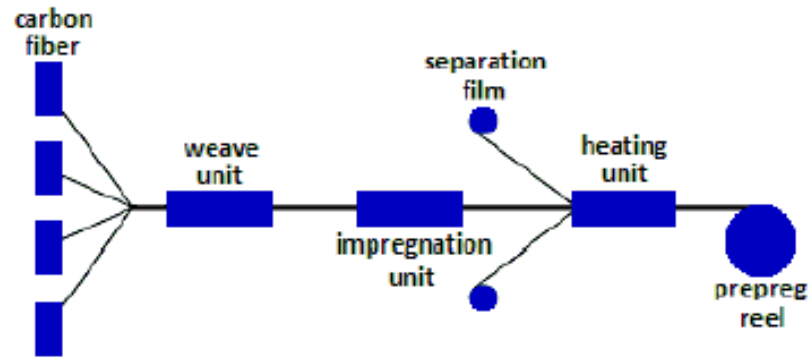

Figure 8: Schematic description of prepreg production and application[24].

As illustrated in Figure 8 a weaving unit produces a fabric out of carbon fibres. This fabric gets then impregnated while being immersed in a resin bath. Before the produced prepregs gets rolled up the upper and lower faces of the impregnated fabric are covered with a film to avoid adhesion between layers. The matrix gets then fixed to the reinforcement with a heating cycle which leads to partial crosslinking of the resin. Storing the prepreg rolls at a lower temperature prohibits further crosslinking and offers successive processing.

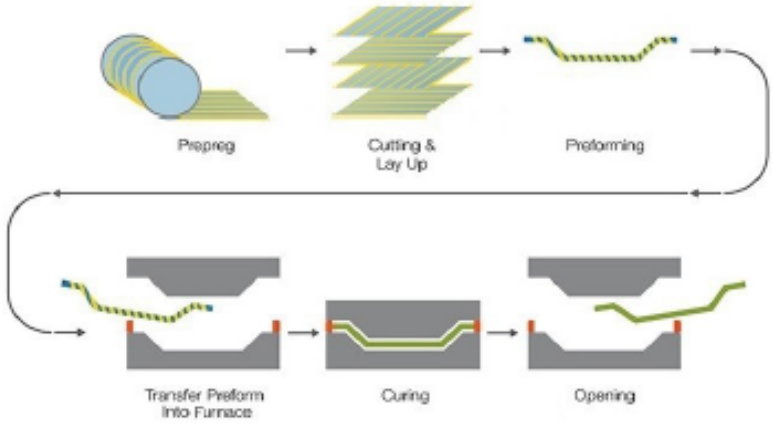

Figure 9: CFRP production by prepreg lamination[24].

By following the succeeding line of action, pictured in Figure 9, a final CFRP product can then be formed from these prepregs. First the prepregs have to be cut to size. After the removal of the release film they can be stacked inside a mould until the desired shape is reached. Following this lamination stage, they have to be packed in a vacuum bag and with an applied vacuum the mould is inserted into an autoclave, where it undergoes a controlled curing cycle while being subjected to pressure, temperature and vacuum simultaneously. The finished product can be extracted as soon as the curing cycle is completed.

As already mentioned, the aim of the curing cycle is that the resin undergoes a full crosslinking reaction that leads to the formation of a macromolecular lattice of infinite size based on covalent bonds. The degree of completion of this process is later responsible for the mechanical properties of the composite, since gaps in the lattice structure can compromise the properties immensely. Therefore, the choice of an adequate heating ramp is important. A favouring factor throughout the process is the fact that the resin initially decreases in viscosity when being subjected to heat, at this stage, aided by vacuum and pressure any voids can be filled and any remaining air or solvents expulsed. After the resin is homogenously distributed, the necessary temperature for the crosslinking reaction can be reached and should be held for a sufficient time to complete the crosslinking reaction.

The mechanical properties of those laminated CFRP materials, being composite materials in general, highly result from their strong anisotropy. They consequently exhibit different mechanical properties in all three directions of space and can be considered as a function of the orientation along which they are measured[26]. Following this reasoning the importance of the fundamental design of a composite has to be highlighted.

Meaning that by an appropriate lamination sequence it is possible to either create materials with nearly isotropic features or tune them optimized into the direction of greater stress. Employing this unique feature CFRP material can be classified in the following categories:

- Unidirectional: all fibres in all laminae are oriented along the same axis
- Angle-ply: laminae are staggered being oriented in a certain angle in respect to each other
- Symmetrical: each sheet is oriented with a certain angle to the plane of symmetry of the laminate
- Balanced: for each sheet oriented with a certain angle in respect to the plane of symmetry of the laminate there is a sheet with the opposite angle
- Quasi-isotropic: properties are approximately equal in all direction of a plane. Obtained by sheets that differ in orientation in a constant angle. The term applies for a least three sheets staggered by 60°.

As already mentioned in chapter 1.1 the strength of a composite depends on the direction of stress and reaches the maximum if the stress if applied into the direction of the reinforcement while having a minimum in the orthogonal direction. In the simplest case, being a lamina with unidirectional fibres and an applied force along this direction the elastic modulus E can be expressed as shown in Equation 1 below.

$$E_1 = \varphi_f E_f + (1 - \varphi_f) E_m$$

Equation 1

where φ_f is the fraction of fibres present, E_f is the elastic modulus of the fibre and E_m is the elastic modulus of the matrix. The modulus is therefore given by the weighted average of the fibre and matrix modulus. Since $E_f \gg E_m$, the equation can be approximated to Equation 2.

$$E_1 \approx \varphi_f E_f$$

Equation 2

The E_1 modulus is therefore directly proportional to the fibre content.

To calculate laminates modulus E_2 in perpendicular direction, the adjacent Equation 3 can be employed.

$$E_2 = \frac{E_f E_m}{\varphi_f E_m + (1 - \varphi_f) E_f}$$

Equation 3

When $E_f \gg E_m$ is considered we establish the next Equation 4.

$$E_2 = \frac{E_m}{(1-\varphi_f)}$$

Equation 4

In conclusion it can be said that the elastic modulus in perpendicular direction is only increased if high quantities of fibres are present.

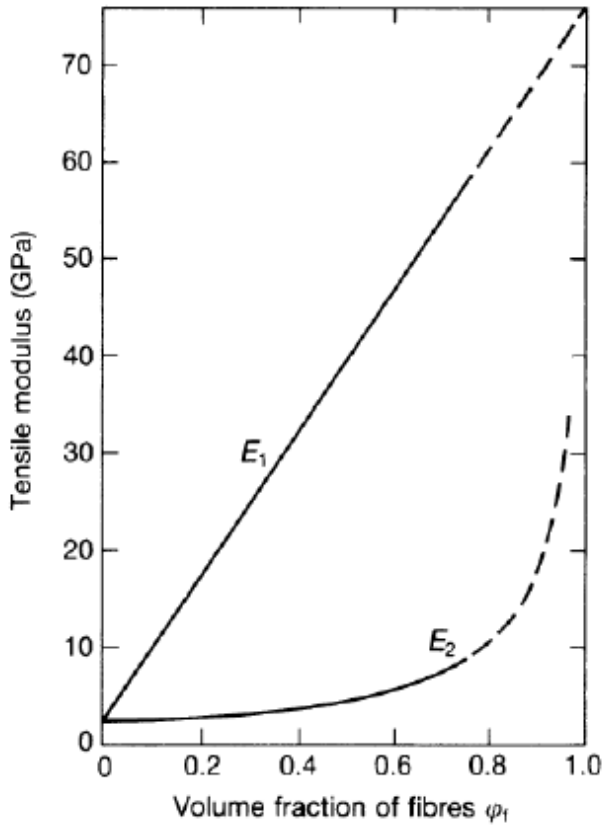

Figure 10: Trend of the elastic modules E_1 and E_2 as a function of the volumetric fraction of fibers φ_f.

The dotted line in Figure 10 represents theoretical values, due to the fact that a high fibre fraction prohibits resin impregnation and thus cannot be utilised. However, Figure 10 shows that E_1 is always greater than E_2 and therefore the mechanical properties in perpendicular direction are always lower. This fact leads to one of the major problems of laminates, delamination.

1.2.3 Drawbacks

Since laminated CFRP is a highly specialised product the advantages have to be paid be a difficult and labour-intensive production process and are therefore relatively expensive compared to classical materials. Furthermore, the fact that if the maximum stress resistance is exceeded once the structure fails immediately to an unrepairable stare. Broken fibres or cracks in the matrix leave the remaining structure with a reduced strength and have to be replaced in order to grand functionality. Another problem is that processes to recycle the material are still under development which makes the regain of usable fibres unfeasible and leaves the operator often with the only choice to waste a material which posts a high load on the environment since it barely decays to its otherwise useful chemical inertness[27].

1.3 Delamination

The most likely type of breakage for laminated composites is the separation between the build in layers, or delamination. Up to 50% loss of strength can be attributed to this phenomenon and along with the fracture resistance it is the biggest problem undermining the long-term reliability of these materials[28]. This event can be caused for example by excessive stress, micro-cracks formed in the matrix to the intrinsic discontinuity of the physical and mechanical properties of adjacent layers[29]. Because the event is caused by hardly detectable anomalies or defects in the structure the breakage occurs at relatively low loads and poses as the biggest thread to laminate composites[30].

1.3.1 Causes

As discussed, failure in laminates arises from defects in the structure which can be at different sites in the structure, at the fibre, at the matrix or at their interfaces. Each of these defects can cause different fracture mechanisms which will be explained in this chapter.

A number of defects, such as voids or resin accumulation, can be caused during the manufacturing process. Voids for example are most commonly found in corners of the structure. The level of porosity depends on various parameters. As illuminated in chapter 1.2.2, the moisture content, the extend and duration of the applied pressure belong to these parameters and if not properly adjusted lead to a loss in mechanical properties. At last also contamination during the layering of prepregs or remaining particles of the release film can cause the same effects and have to be avoided[31].

When the resin is cured well and the composite obtains his final properties as a solid further mechanical processing can lead to micro-cracks in the matrix, which can later on, during the lifetime of the material, lead to fractures or detachment between reinforcement and matrix if interface tension becomes too high. Another problem following detachment formation is the entry of water or humidity inside the composite leading to further degradation and possible failure[32].

The final collapse of the structure is usually a result of the combination of the before told effects and the subjection of the material to cyclic loads, strong temperature changes or impacts.

1.3.2 Crack propagation

As elaborated in the previous chapter 1.3 the defects present can lead to breakage or delamination. Starting regularly at the edges of laminates or around bolts and rivet holes this phenomenon occurs at points which bear the highest stress in the material. The resulting crack propagation can be explained by the following mechanism[33]. When increasing stress is applied to the material, initially both matrix and reinforcement deform plastically. But with increasing stress first the matrix deforms plastically and later on also the reinforcing fibres until the matrix collapses and the delamination begins. It is evident from micrographic studies that the cracks will not propagate through the fibres and follow the interface between fibre and matrix instead[34].

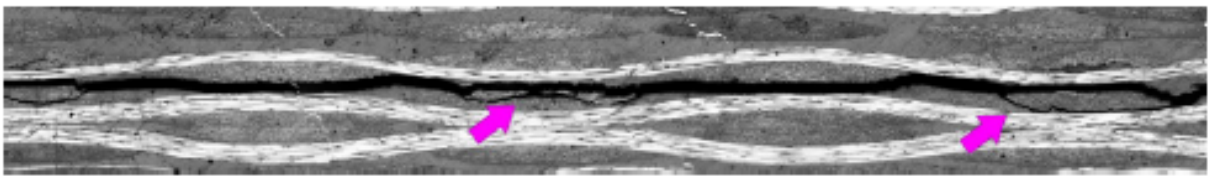

Figure 11: Micrography of linear crack propagation between matrix and fibrous reinforcement (deviations marked with purple arrows)[34].

This behaviour, depicted in Figure 11, is due to the fact that the crack follows the path of least resistance which is the layer of pure matrix between laminates which possesses the lower mechanical properties compared to the fibres which will not be crossed by the crack.

1.3.3 Toughening

As it is apparent by now this predicament prohibits the use of laminated composites for critical application and therefore the materials resistance towards delamination has to be improved, which will then lead conversely to a broadening of the application

range. In order to develop effective solutions a method to measure the fracture toughness of the material has to be established. Delamination studies are conducted with a system of two superimposed elastic beams and they differ according to the way in which the forces are applied. In Mode I the applied stress is perpendicular to the crack plane, while in Mode II the stress is applied parallel to the crack plane and drags the beams along each other, in a way comparable to a sliding motion[35]. The mentioned modes are illustrated in the following Figure 12.

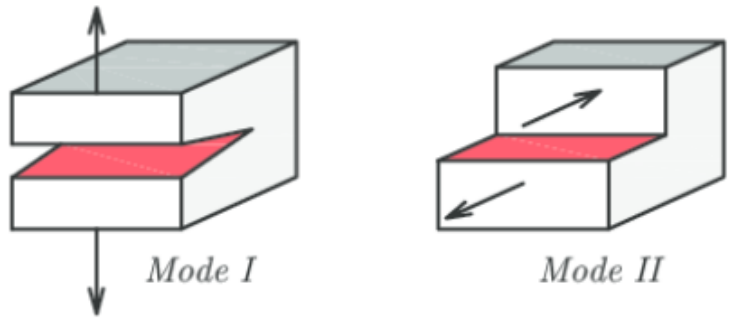

Figure 12: Different modes of delamination testing[36].

Mode I can be tested with the, so called, Dual Cantilever Beam (DCB) test, while Mode II is tested with the End Notched Flexure (ENF) test. Both of these tests were developed to study the increase of delamination resistance based on the goal of toughening of thermosetting matrices whilst leaving the mechanical properties unchanged. Attempts to reach this goal have been made by adding rubbery materials with a good degree of crystallinity, creating heterophasic systems[37]. The appropriate toughener has to be chosen due to a high compatibility with the matrix.

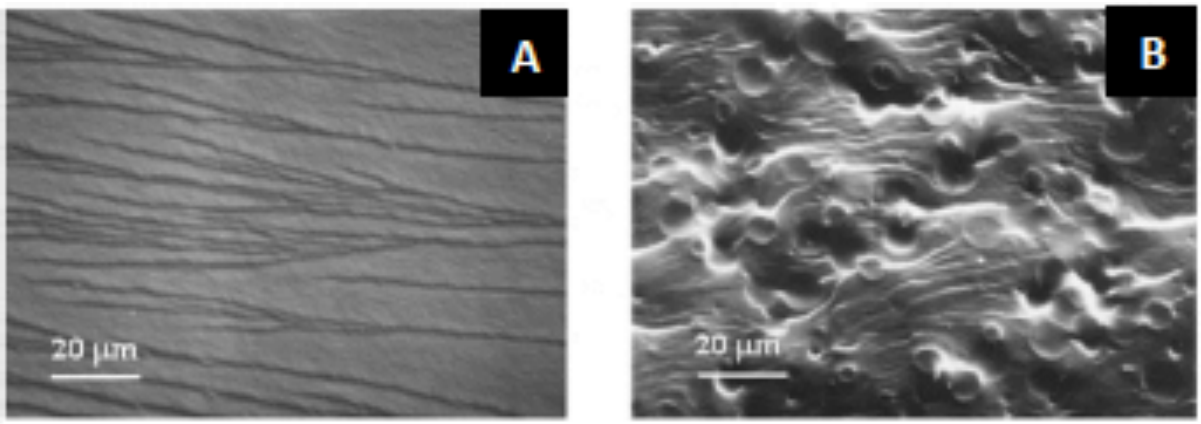

Figure 13: (A) Failure surface of the pure matrix; (B) Fracture of the toughened matrix[37].

Figure 13 reveals that a crack in a unmodified resin leaves a smoother surface in comparison with a crack in a modified matrix, because localized yielding phenomena delay

the fracture process causing an increase in toughness evidenced by this, so called, ductile fracture. Following this train of thought, many reinforcement methods introducing toughening particles in the matrix layers between fibrous layers have been used. Yun et al. for instance show in their work that the addition of polysulfone particles (PSF) in CFRP with epoxy resin increases the fracture resistance of the matrix by 220% in relation to the virgin material[38]. The same group also conducted a study of the interleaving with a PSF film instead of particles giving rise to an increased toughening effect. The influence of the thickness of an added polyethylene film on the interlaminar fracture in Mode I was tested by Matsuda et al., observing a correlating increase of the resulting fracture resistance with an increase of thickness up to a point from which on the added layer acts like a continuous layer of additional reinforcement[39].

An advancement in this field of studies lead recently to an interest in nanofibrous fabrics as toughening material.

1.4 Nanofibers

Nanofibers, in comparison to the material in conventional form, have the advantage of a high surface to volume ratio on the one hand which can enhance their embedding and adhesion in the matrix and on the other hand their maximized flexibility and strength. Furthermore, the addition of nanofibrous reinforcements imposes a negligible effect on the thickness and weight of the specimen, leaving the beneficial properties of the composite unaltered. The nanofibers increase the fracture resistance mainly by being an obstacle for a propagating crack to overcome. A second effect is the distribution of stress concentration[40]. The modification of interlayers between prepregs with nanofibrous membranes was initially patented by Dzenis and Reneker [41]. They proposed the utilisation of a polymeric nanofibrous membrane produced by electrospinning and managed to observe a consistent increase in delamination resistance. A 280% increase in Mode I toughness was achieved with the modification of PSF in the form of nanofibers by Li et al. [42]. Zhang et al. optimised the production parameters of polycaprolactone (PCL), polyvinylidene fluoride (PVDF) and polyacrylonitrile (PAN) nanofibers, testing their mechanical reinforcement properties by Dynamic Mechanical Thermal Analysis (DMTA)[40]. They established that the best increase in Mode I fracture resistance was obtained by starting from a 15% wt solution of PCL, which yielded a delamination resistance of the modified composite 92% higher than that of the virgin material. An increase of static fracture resistance by 124% and a decrease of fatigue

by 96%, both tested in Mode I, was observed after the addition of Nylon 6,6 nanofibers by Brugo et al.[43].

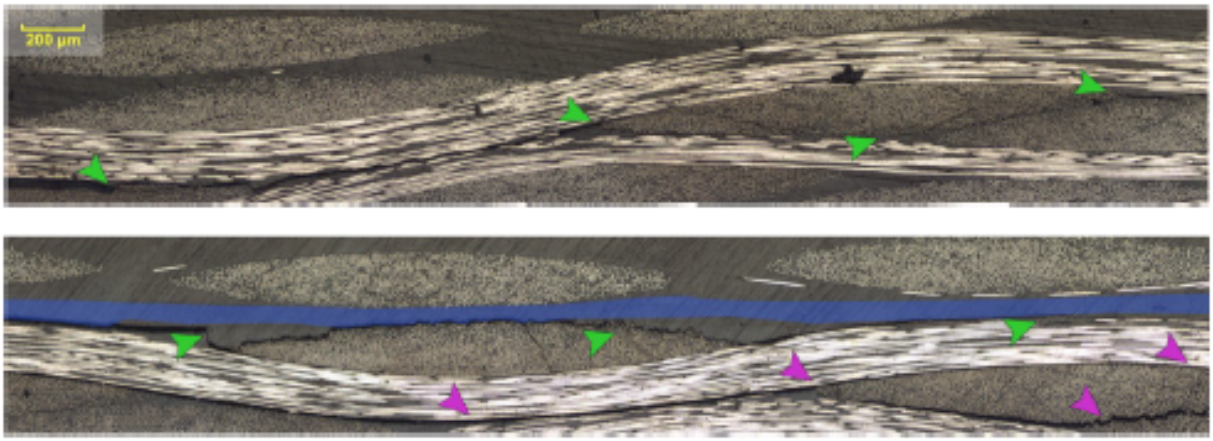

Figure 14: Micrographs show the difference in crack propagation between virgin material (up) and a specimen modified with a nanofibrous membrane, visualized in blue, (down). The green arrows show the main fractures, while the purple ones show the secondary fractures imposed by the presence of nanofibers [43].

To illuminate the benefit of reinforcement by nanofibers further, Figure 14 reveals that a successful modification increases the toughness of the matrix by such a degree that it exceeds the toughness of the reinforcing fibres. This can lead to a crack propagation not only in the pure matrix layer but instead causing the crack to pass through the different layers in a zig-zag movement rising the energy necessary for a crack to penetrate a structure. Brugo et al. evaluated the influence of the thickness of nanofibrous membranes and the thickness and diameter of the fibres[34]. They showed in Mode I DCB tests that an increase in membrane thickness leads to a decrease in fracture strength, but ENF studies for Mode II failure exhibited that membrane thickness has no significant effect on the composite performance. DCB studies regarding the orientation showed that randomly oriented fibres facilitate a better resin impregnation than aligned fibres, increasing the reinforcement effect. The studies of the diameter show that an increase in the diameter of the fibres lowers their reinforcement capabilities but increases the ability to absorb a higher energy stepping up the fracture resistance.

The above-mentioned works show that nanofibrous membranes bear many opportunities to improve CFRP material, due to their capability to be precisely tailored to their application.

1.4.1 Damping

The downside of the high stiffness of CFRP material is the brittleness, which can be addressed with the discussed toughening methods. Next to the brittleness, CFRPs materials are known for their propagation of vibrations, which can lead to fatigue, crack formation and at the least to a high noise for instance in automotive or aeronautical applications[44]. The oppositional property is the ability to dampen vibrations without propagating them or damping capacity. Recently this property enjoys a growing interest and its improvement is studied intensively[45].

Vibrations are defined as mechanical oscillations of a system displaced from its mechanical equilibrium position. Depending on the inherit material properties, the geometry and the environmental conditions each object has a different response to mechanical stress. CFRP originally have a low damping capacity and therefore need to be modified in order to supress vibrations effectively[46]. Their damping capacity, adding up to the anisotropic properties of CFRP can be maximised to some extend by clever structural design and are at a minimum in the direction of the fibres and reach a maximum in the transverse direction[47].

Methods applied to increase the damping capacity can be divided into active and passive damping systems. Active system being aided with external mechanisms or devices, involving sensoric monitoring or vibrational stress in real time and reacting with an instant active response to counteract the vibrations. While these systems have the advantage of enabling an instantaneous response it hardly justifies the complexity and additional weight of equipment that is required. Despite these drawbacks this approach remains the optimum solution for applications which require immediate and adjustable damping. Passive systems on the contrary are based on the principle of dissipating the stress energy. This can be achieved by the integration of a viscoelastic damping material into the composite structure. The final result should be similar to active systems, namely the reduction of the disturbance effects of vibrations, with an increase in structural stability. The passive approach being more energetically and economically efficient requires a high understanding of the structure and a clever design applying the modifications in the appropriate extent to the adequate regions in the final structure.

Since the incorporation of viscoelastic materials into the composite rather than deposing it on the surface has a stronger effect on the damping capacity this approach is

studied most. Introducing damping material, however, can generate a reduction in stiffness and structural resistance, differing from case to case [48]. Viscoelastic materials, which get their name from behaving viscous and elastic simultaneously, have the ability to dissipate vibrational energy in the form of heat when they undergo deformation. The models applied to study the viscoelastic properties of these materials are based on the assumption that the system holds one purely elastic component, which describes a reversible deformation and one which behaves purely viscous, resulting in an irreversible deformation. Averaging the two results can then be considered the overall behaviour of the system. A number of methods have been developed in attempt to explain viscoelasticity.

Figure 15: Schematic representation of the Maxwell viscoelastic deformation[49].

Starting with Maxwell´s model, outlined in Figure 15, describes viscoelastic materials as behaving elastically over short time intervals and viscously or longer time intervals can be represented by viscous heatsink (η), described as a Newton element, connected to a spring (E), described as a Hook element, and is usually applied to study systems in which small deformations occur. In Maxwells reasoning the system, subjected to a constant stress (σ), will first deform in an elastic way, which will relax fully upon release. If the stress is applied over a longer period of time the viscous part starts to deform gradually and irreversibly. This model predicts an exponential decay of the stress lasting on the sample. However, this system does not accurately describe the creep inside the material. For a more accurate approximation for solid viscoelastic materials the Kelvin-Voigt model can be employed varying to Maxwells approach by connecting the Newtonian damper in parallel with the spring, as shown in Figure 16[27].

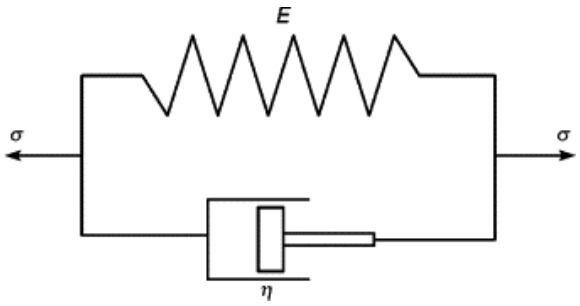

Figure 16: Schematic representation of the Kelvin-Voigt viscoelastic deformation[49].

Because of the parallel arrangement, the two elements undergo the same deformation. Meaning that for a constant applied stress the deformation rate decreases over time. Stress relaxation can be further analysed in a stress/deformation curve of a cyclically loaded specimen.

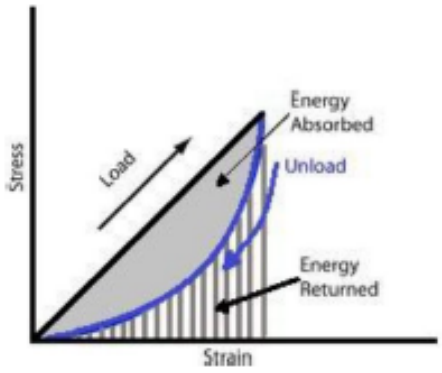

Figure 17: Stress-strain curve of viscoelastic material[24].

Figure 17 shows that a specimen when initially subjected to a load cycle deforms and energy is stored. Upon relaxation the deformation decreases while the stored energy is released in form of heat. This energy can be quantified by integration of the area below the curve. Viscoelastic materials show a delay while returning to their original shape due to the loss in energy by heat. This part of the lost energy can be attributed to the viscous and irreversible deformation leaving the system altered with a shift in its centre of gravity[50]. For further characterisation two moduli are introduced. The conservative modulus (E´) relates to the elastic behaviour and measures the stored energy. E´´, the dissipative modulus, describes the viscous behaviour and is quantified by the dissipated heat energy. The ratio between both of these moduli, describes the damping capacity of a material and will be further addressed as “loss factor”, generally indicated by $tan\delta$. The loss factor is described by the following Equation 5.

$$tan\delta = \frac{E''}{E'}$$

Equation 5: Description of the loss factor

Aluminium for example, while having a similar E´ to CFRP possesses a higher loss factor due to a higher E´´ and therefore exhibits a better vibration dissipation capacity. Probing of the damping capacity can be conducted utilizing Dynamic Mechanical Analysis (DMA) which will be later detailed in chapter 0.

1.5 Electrospinning

Electrospinning is a production method for membranes, or rather, nonwoven mats that have a significant surface area, high porosity and very small diameters in the nanometre scale. These properties allow their use in various applications, such as nano and micro-filtration, scaffolding for tissue engineering, flame retardant applications and reinforcement of composite materials[51]. Due to the superior ability to use a wide range of polymers, compared to traditional techniques (exp. dry spinning, melt spinning, etc.) and the fact that the resulting diameters lie in the nanometre regime, this technique became subject of a growing interest over the last 20 years despite that evidence of the first applications of electrospinning, called electrostatic spinning at the time, date back to the early 1900s. It then appears in a first patent by Formhals in 1934, who developed over the years a machine being able to produce fine fibres[52]. Adding up to the number of researches dedicated to the topic the name Taylor should be mentioned who studied the deformation of solution drops at the tip of a needle subjected to an electric field in the 1960s[53]. He deduced the value of the opening angle of the cone that forms which henceforth got the name Taylor cone.

During the process a polymeric solution gets pushed through a glass syringe that acts as a reservoir for the polymeric solution and is connected, via Teflon tubing, to a metallic needle. The applied voltage between the needle and the collector surface, either a drum or a screen, guides the exiting solution from the needle to the collector. The collector usually being a metal plate or a rotating metal cylinder. Depending on the desired orientation of fibres. The named components can be found in the following Figure 18.

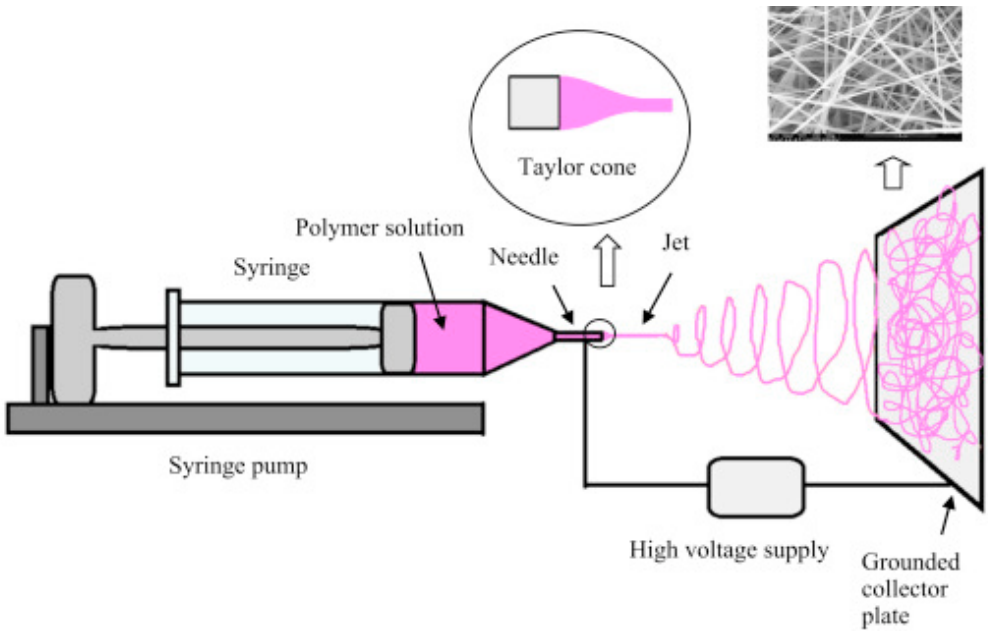

Figure 18: Electrospinning setup[54].

The important detail concerning the path of the solution is that due to the surface tension and the intrinsic cohesive forces the polymeric solution, while being ejected, forms a drop at the tip of the needle. If a potential is applied the drop starts to deform, following the electromagnetic field, passing a spherical shape into a conical shape, the before mentioned Tayler-cone, until the cohesion forces succumb to the pull of the electrostatic field reaching a solution specific critical potential and the solution starts to leave the drop forming a jet, see Figure 19 below.

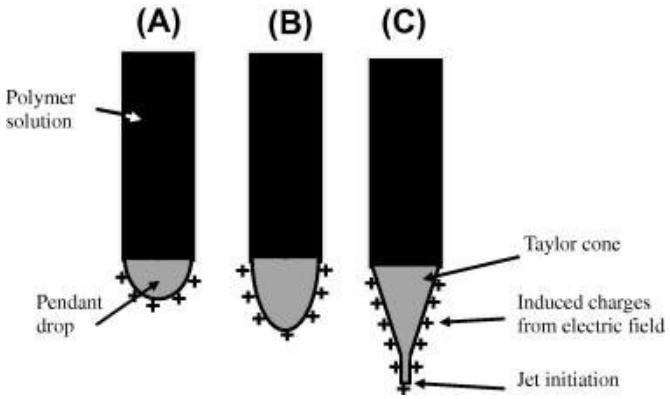

Figure 19: Schematic description of Taylor cone formation[55].

After its initially linear pathway the trajectory of the jet changes into a spiral pattern, visualized in Figure 20, which widens and destabilizes with distance. During the jets widening path the diameter of the ejecting flow decreases while the surface area increases, leading to a complete solvent evaporation before the final fibres are conceived on the collectors surface [56,57].

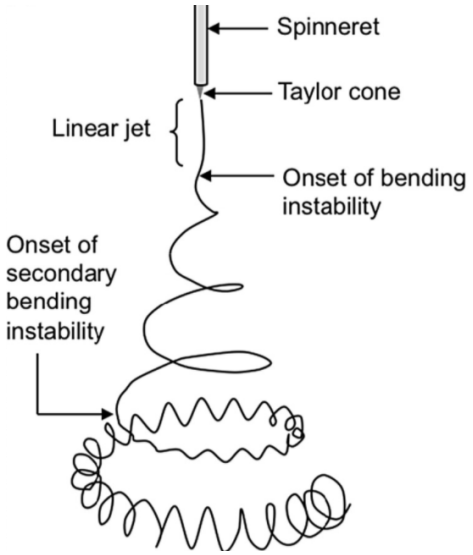

Figure 20: Schematic representation of jet[58].

Processing and the quality of the fibres are influenced by solution parameters, including viscosity, solvent volatility and conductivity leading to difficulties in jet formation and the regularity of the final shape of the fibres. These solution parameters depend on the

polymer concentration and solvent properties. Low viscosity favours the ejection of a spray, rather than a jet, producing drops instead of fibres[59]. This effect is referred to as electro nebulisation, which is employed in techniques such as electro spray ionization for mass spectroscopy is visualised in Figure 21 (A)[60]. If the solutions viscosity is just slightly to lower than ideal, the fibres show swellings, called beads, which are lumps of polymer affecting the fibres quality. Beads are shown in Figure 21 (B). A high viscose solution, due to high polymer concentration, results in a thicker fibre diameter and can lead to solidification inside the needle and block the ejection[61].

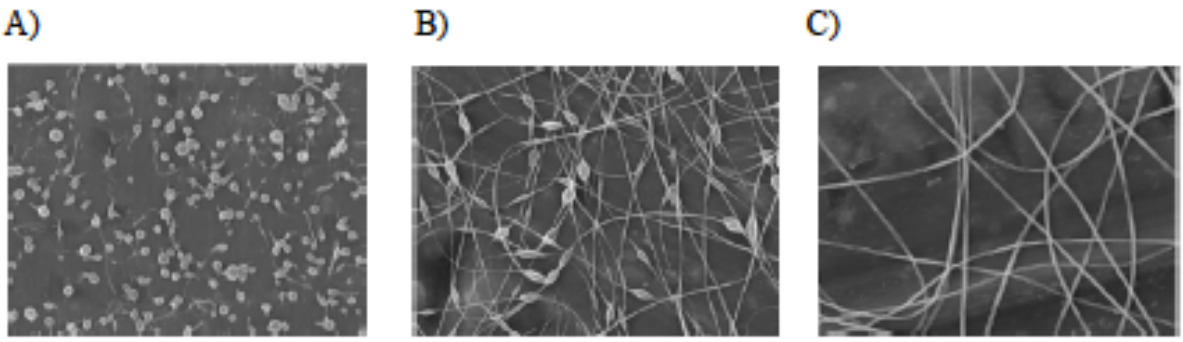

Figure 21: Scanning electron microscopy images showing the influence of concentration on the production: Electrospray (A); Fibres with beads (B); Continuous fibres (C).

Since polymers are good insulators the conductivity necessary for the process is only a property of the solvent[57]. Following these facts, the solution parameters have to be tuned carefully and in relation to the existing environmental parameters, most importantly being temperature and relative humidity[62]. Process parameters, such as applied voltage and distance from needle tip to collector have to be chosen accordingly. While it is proven that the applied voltage needs to exceed a certain threshold value for the Taylor cone to form, its impact on the diameter of the fibres stands still to discussion. While Zhang et al. concluded that an increase of voltage would result in a thickening of the fibres, the group of Yuang et al. established that the repulsive forces in the jet producing thinner fibres in the end[63]. Deduced from that, one can be sure that the parameters have to be optimised to each application. The distance from needle to collector, for instance, not only dictates the electric field strength necessary to enable the process but it also stands in relation with the flight time and is consequently responsible for the stretching of the fibres and the completion of the solvent evaporation[64]. Another influencing factor is the diameter of the needle that favours the formation of thinner fibres, however it also favours the likelihood of a blockage when solutions with a high viscosity are run through it[65].

1.6 Scanning Electron Microscopy (SEM)

As already applied in chapter 1.5 Scanning Electron Microscopy (SEM) is an effective mean used to characterise nanofibers. During a SEM experiment a solid sample gets targeted by a stream of primary electrons from the instrument, sourced from a tungsten filament. The detection is done by scanning the excited sample detecting the emitted secondary electrons. By scanning the sample in small steps, a significant reduction in noise is achieved compared to the imaging of a vast area at once[66]. While the technique was developed in 1935 by Max Knoll, improving it since leads to a resolution range from 1-10nm for modern instruments[67]. Along with the fact that SEM allows a better depth resolution compared to other imaging techniques it proves to be useful to investigate nanofibrous structures. A more detailed representation of the instrument setup can be found in Figure 22 below.

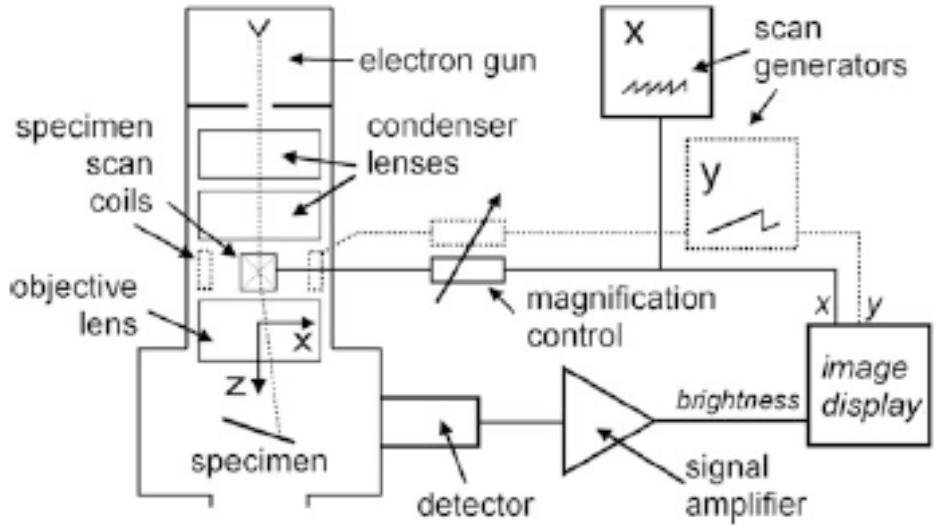

Figure 22: Schematic representation of a scanning electron microscope[66].

To avoid artifacts and defects in the images the method is carried out under vacuum, to maintain stability for the sample itself it needs to be prepared to withstand the vacuum and also the electron beam its subjected to. For non-metallic samples electric conductivity has to be established in addition. For these purposes nonconductive samples have to be dried beforehand and then coated by conductive materials, such as platinum, chromium, iridium or graphite. The most commonly used coating is an alloy of gold and palladium[68].

1.7 Differential Scanning Calorimetry (DSC)

Differential Scanning Calorimetry (DSC) allows us to obtain information on the materials thermodynamics of solid or liquid phase transitions, that produce or absorb heat, by heating or cooling it in a controlled manner[69]. The technique is based on measuring the difference between the heat flow of the sample and the reference when the temperature is varied at a constant rate. The difference in the heat flow between the two is due to phenomena occurring in the sample, such as the glass transition, crystallization, melting, etc. and can therefore be used to asses these phenomena[61]. When the samples are both subjected to a continuously rising input of energy in form of heat the reference will show a direct warming linear to the corresponding input energy while the sample will heat up slower while an endothermic event occurs and will consequently warm up faster during an exothermic event.

1.8 Dynamic mechanical analysis (DMA)

Dynamic mechanical analysis, also called dynamic mechanical spectroscopy, utilises a sinusoidal stress (σ) to deform the sample and monitor the materials response[70]. The deformation can be referred to as strain at carries the letter γ. The materials response is highly influenced by the temperature present. DMA is used to probe a wide range of materials for their changes in a number of physical properties, such as volume, enthalpy, heat capacity, thermal expansion, the storage modulus (E´), the loss modulus (E´´) and the loss factor ($\tan\delta$)[71]. These properties depend on the materials tendency to flow, meaning viscosity that can be calculated from the phase lag and stiffness from the sample recovery. Deduced from that an understanding of the materials ability to disperse energy in the form as heat, meaning damping and the ability to recover from deformation, meaning elasticity can be gained. Traditional techniques fail to keep up with the ability of the DMA to measure a materials response continuously over a temperature range[72]. Mapping modulus or viscosity as a function of temperature would require the conduction of a statistically appropriate number of experiments equilibrated at the desired temperature and is therefore excessively more labour intensive and less accurate.

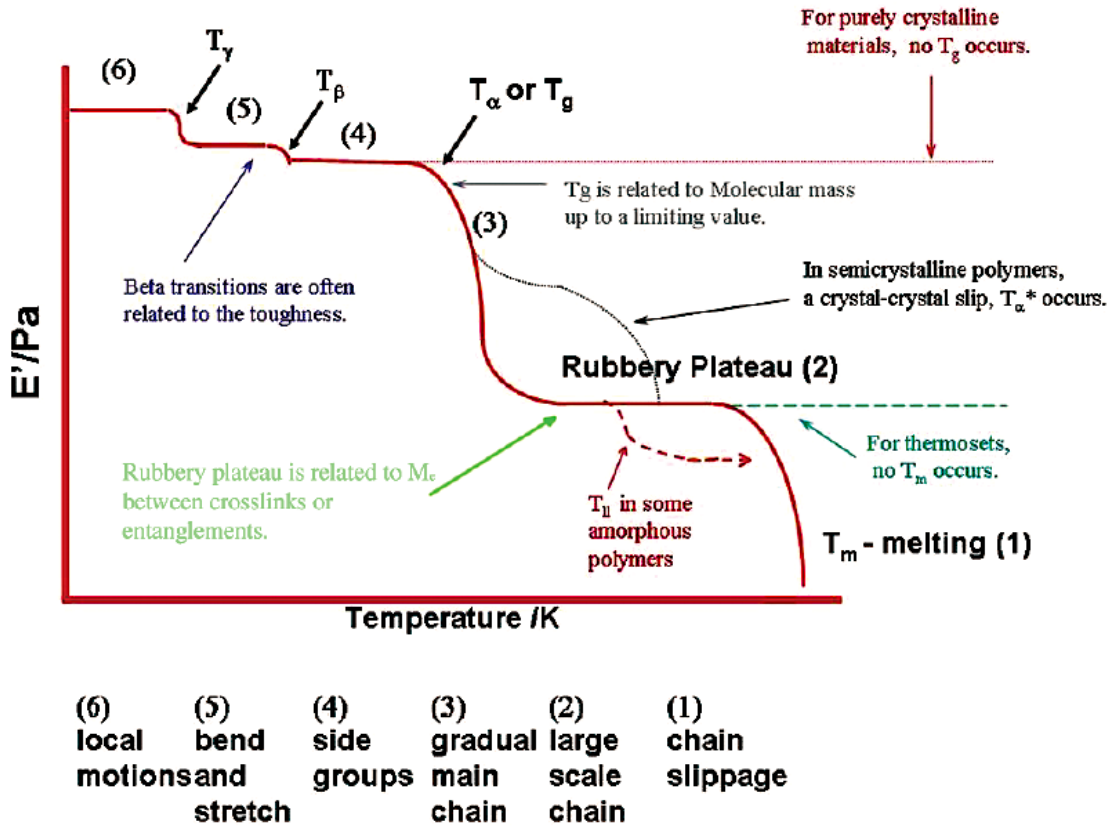

Figure 23: Full overview of thermal events present in a DMA temperature-time scan for E´ as a function of temperature[73].

The most important event that is probed with this method is the glass transition temperature T_g, which marks the change of a polymer from a glassy, solid behaviour to a rubbery one. Due to the fact that DMA is more sensitive to these phase changes than other employed techniques such as DSC or thermomechanical analysis (TMA) it is possible to determine the operating range of a polymer in higher detail, as can be seen in Figure 23[74]. In the temperature region below T_g over transitions can become apparent in DMA measurements. They correspond to gradual chain movements or other changes in molecular motions often associated with side chain movements and play a role for the toughness of the material[75]. The relation of sub-T_g transitions to vibrational and acoustical damping has also been proven by Nelson at al. and are therefore important for this project[76,77]. The labels for these transitions are given backwards from the glass transition temperature by $T\alpha$, $T\beta$, etc. In the range of these lower transitions possesses the stiffness to resist deformation and the flexibility to resist breakage under strain[72]. While the sub-T_g transitions are responsible for the materials properties in the glassy state the “rubbery plateau” after the T_g is associated with the degree of crystallinity in a material[78]. The melting point T_m marks the end or terminal region of these transitions and corresponds to the material in a molten state, when the polymer chains

of the material can slide past each other and the able to flow as freely as the molecular weight of the polymer allows. After T_m is exceeded the polymer structure undergoes degradation influenced by environmental effects. At this point highly crosslinked polymers will degrade directly as they are not able to melt. Other polymers either degrade by crosslinking or by chain scissoring differing widely in their appearance, viscosity elasticity and stability[72].

Another advantage of the superior sensitivity of DMA is its resulting ability to probe thin coatings, highly crosslinked thermosets and recently even powders for their T_g[79]. Over the years the study of materials in nonstandard environments become more and more common and so knowledge about the effect of solvent contact, humidity levels and UV exposure could be obtained[80], which widens the application range up to the field of food analysis for instance.

The commonly used forced resonance analysers are designed to force the sample to oscillate at a fixed frequency and are therefore well able to scan a material for its performance across a temperature range.

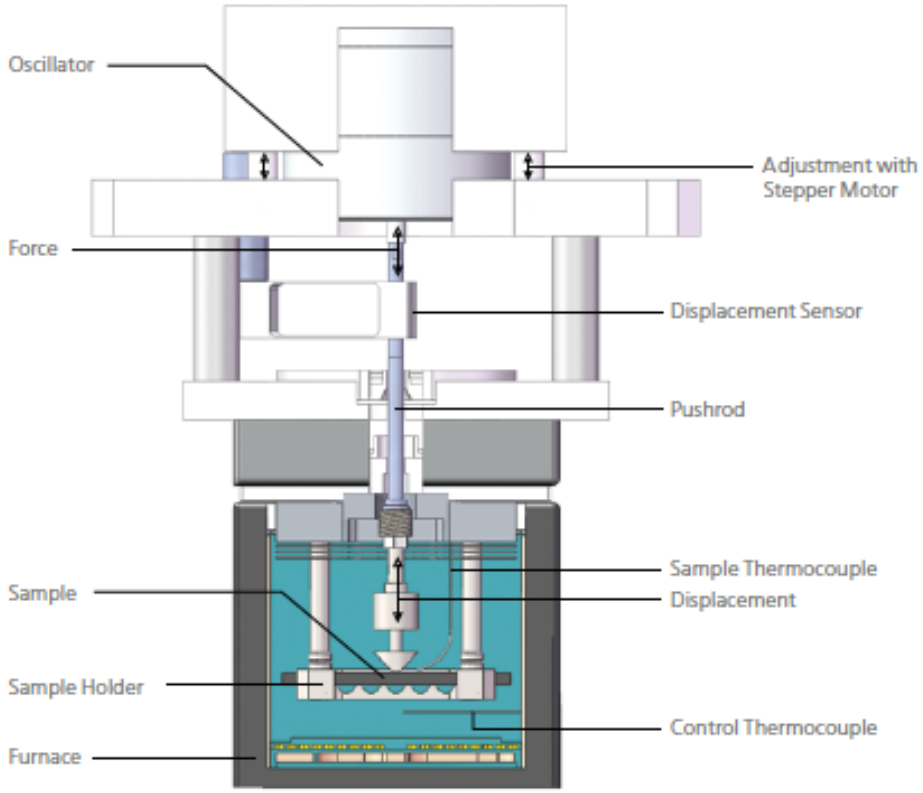

Figure 24: Schematic depiction of a common DMA instrument[81].

As in Figure 24 above pictured, an instrument consists of several parts that control the deformation, the temperature, the sample geometry and its environment. The furnace

enclosing the whole apparatus has been left out of the scheme to aid clarity. A Linear Vertical Differential Transformer (LVDT) measures displacement by detection of a change in voltage that is caused by the sample moving through a magnetic core.

While there are different types of bending and flexing fixtures commonly used in DMA analysis the simplest and most straight forward is the three-point bending fixture[72].

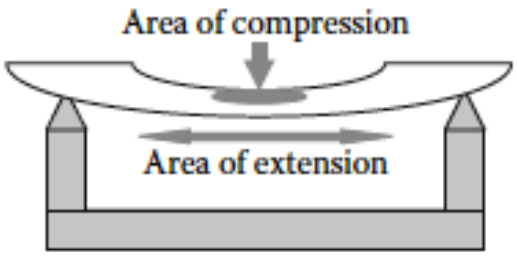

Figure 25: Schematic depiction of the three-point bending fixture for DMA analysis[72].

Figure 25 above explains how a deformation in flexure mode is built from the combination of an extension and a compression strain. A sample fit for three-point bending should be able to pivot freely throughout the experiment and therefore overlap the span on each end and be of uniform diameter. The volume of the sample dictates the time necessary for the sample to be equalised at a certain temperature during the experiment due to its heat capacity.

DMA experiments can be conducted as temperature-time studies, frequency studies or to obtain dynamic stress-strain curves. Temperature-time scans, being the technique applied in this project, vary the temperature over time while the applied frequency is constant. The choice of applied frequency alters the results quantitively, since higher frequencies induce more elastic behaviour. Lowering the frequency will therefore shift the temperature of a transition to a lower temperature. The best approach to choose a suitable frequency is to simulate the specimen's environmental conditions. However since many industries have their own standards the experimental conditions are commonly matched to military-specifications, an ASTM-Standard or a specifical industrial test[72].

Since many commercial polymers contain blend-in modifiers and fillers, DMA has been used to examine their effects on the bulk properties of the polymer, which leads to the scope of this project.

2 Scope of the project

The fact that carbon fibre composite materials possess excellent mechanical properties, equal to or even exceeding those of conventional substances (metals, ceramics, etc.), combined with their low density, allows a reduction of weight for many established products. This characteristic helps in the aerospace, automotive and sports industry to push the limits on speed, reach and minimum fuel consumption.

But the high mechanical strength and stiffness goes hand in hand with the brittleness of the material. Furthermore, the stiffness is also responsible for the fact that vibrations are easily propagated through the material. This not only lowers the comfort for applications in the leisure sector due to high noise and vibrations, this is for example a drawback for composites application in vehicles. The propagation of vibrations also leads to degradation and structural failure of the material even when subjected to relatively low forces. Indeed, microcracks originate in the matrix layer between the carbon fibre sheets since the polymer (often thermoset for advanced applications) is the most susceptible to the vibrations damage. Cracks, once formed, can easily propagate in the matrix phase and will finally cause breakage of the composite between its layers. Therefore, the damping of vibrations is not only important for the improvement of comfort in applications but also to reduce the risk of delamination and fatigue of the composite, improving also the lifetime and consequently broadening the field of applications.

A lead on how to improve the ability of CFRP to absorb vibrational energy induced by external stress has been established by the same research group this project is carried out in. The studies conducted have shown that the addition of nanofibrous membranes, made up by a blend of nitrile butadiene rubber (NBR) and Poly-(ε-caprolactone) (PCL), incorporated between sheets at the lamination phase of CFRP production increasing damping and also strengthens the matrix phase to hamper delamination.

The aim of this present work is to expand these preliminary findings and to evaluate the effect of number, position and thickness of layer modifications in the composite with regard to the damping behaviour and consequently the resistance to delamination and fatigue. During this project fibrous membranes are produced, characterised by SEM and DSC before they are introduced into the composite during the lamination. The complete composite then gets probed for damping behaviour by means of DMA. Finally, the results will lead to a suggestion of an optimised stacking sequence.

3 Results

3.1 Specifications of polymer blend for nanofiber production

The polymeric mixture chosen for the later production of nanofibers is made up to 60%wt by Nitrile Butadiene Rubber (NBR) and to 40%wt by Poly-(ε-caprolactone) (PCL), based on previous work on the optimisation of the fibre composition with respect to their impact on CFRP behaviour[82].

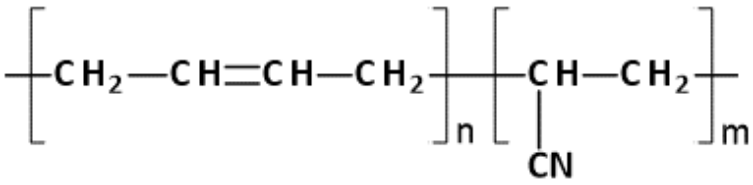

Figure 26: Monomeric structure of nitrile butadiene rubber[83].

NBR, pictured in Figure 26, is a copolymer combined from acrylonitrile and polybutadiene. Polybutadiene was one of the first elastomers invented to mimic natural rubber and the most prominent attributes are the low T_g at -106°C, low air permeability and resistance to aging. Acrylonitrile is a derivative of acrylic acid and has the asset of a CN group which lowers permeability of oils and hydrocarbons[84]. When the two monomers are combined with an excess of butadiene and further crosslinked, the overall behaviour of the resulting material is elastomeric. Due to its excellent properties NBR rose to a central role in the rubber industry over the past years and is commonly applied. Although there are ways to influence the copolymers properties by variation of the relative monomers content, I want to focus more on the blend which is used in this project.

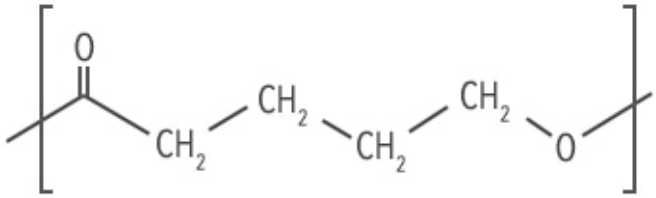

Figure 27: Structure of Poly-(ε-caprolactone) (PCL)[85].

PCL, the second constituent in the polymeric mixture (Figure 27), is a synthetic biodegradable polyester, which finds itself commonly applied in applications demanding biocompatibility. Reasonable thermal stability, excellent processability due to a low viscosity and good solvent resistance in general are properties which elevate interest in PCL on an industrial level[86]. More in detail: The T_g of PCL lies at -60°C, the melting

temperature at T_m = 60°C and it decomposes at 360°C[87]. Therefore, the semicrystalline polymer can undergo viscoelastic deformation and can creep at room temperature.

In order to electrospin a polymer, it is necessary to solubilize it first. This holds true, even when different polymers have to be electrospun in the same mixture, with the complication of finding a solvent, or better a solvent system, that is able to dissolve both polymers at the same time and guarantee properties that are compliant with the electrospinning process requirements (i.e. convenient conductivity and rate of volatilisation, suitable final solution viscosity, etc.). The appropriate mass percentages and solvent systems have been established by the group in preliminary works and will be named in paragraph 5.2.

NBR was chosen due to the rubbery characteristics it inherits. However, its T_g, considerably lower than room temperature, determines produced nanofibers, only made up by this component, to creep over time, leading to the formation of a compact film. The images, in Figure 28, show that nanofibers membranes from 100% NBR lose their fibrous structure quickly.

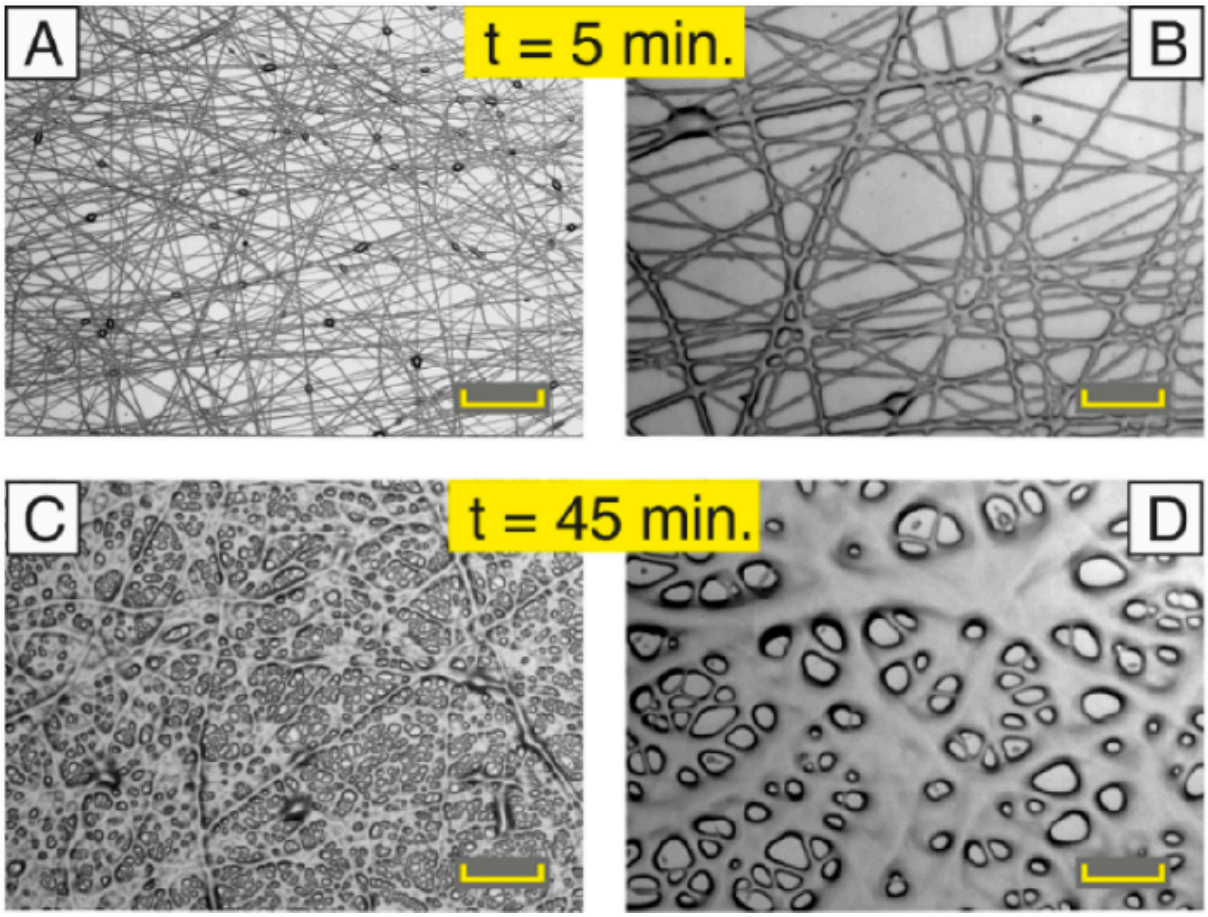

Figure 28: Electrospun nanofibers from 10%wt NBR solution in DMAc (S-NBR). Nanofibers after 5 min (A, B) and after 45 min (C, D) of deposition. Scale bar: (A, C) 50µm; (B, D) 10µm[82].

PCL is blended into the compound to fabricate dimensionally stable fibres at room temperature. The weight ratio of 60/40 of NBR and PCL has proven to raise up suitable nanofibers for damping, as can be seen in Figure 29.

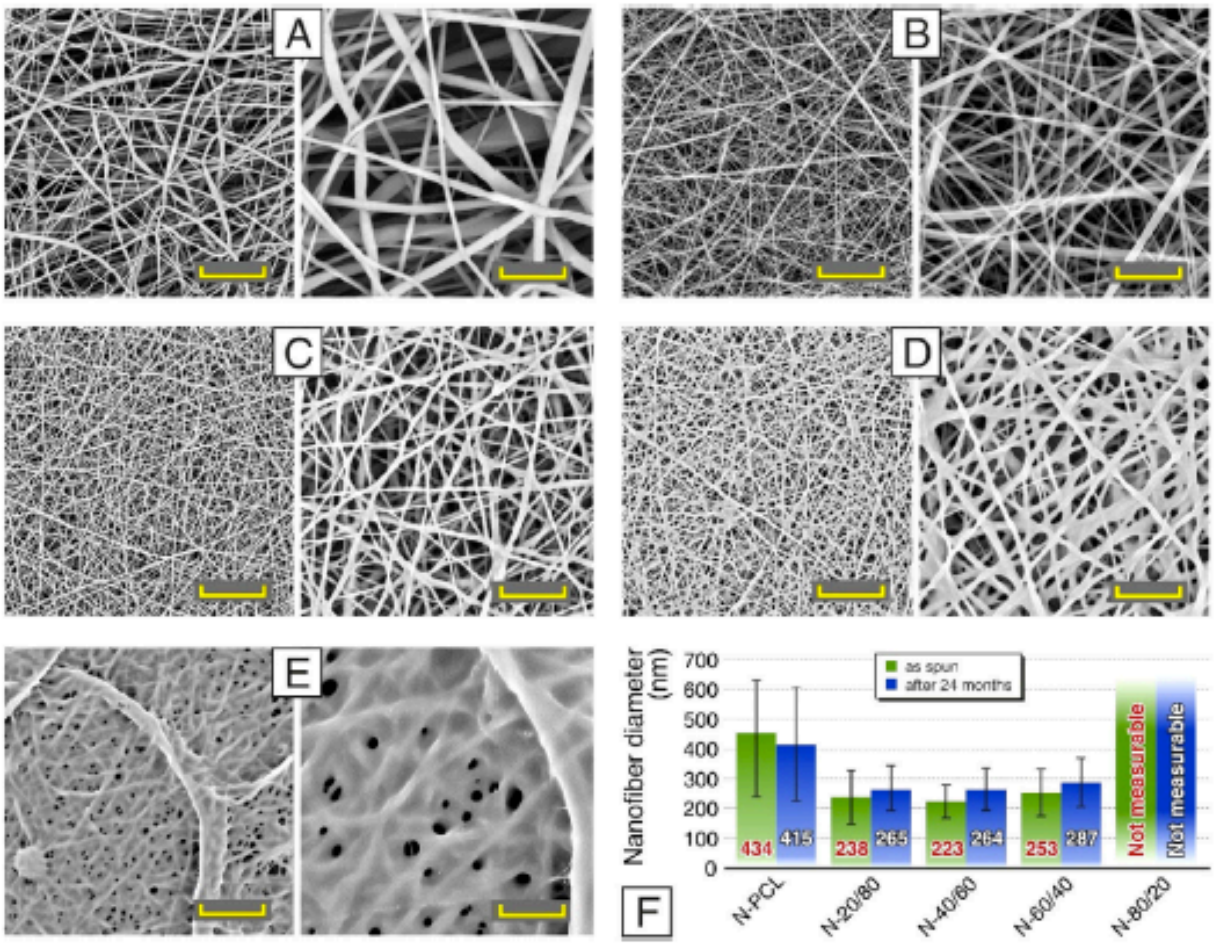

Figure 29: SEM images of nanofibrous mats: A) N-PCL, B) N-20/80, C) N-40/60, D) N-60/40, E) N-80/20. Scale bar: left (5000×) 12µm, right (15,000×) 4µm. F) comparison of the average fibre[82].

Due to the fast solvent evaporation during the electrospinning process, the homogenous polymeric solution becomes frozen into a single-phase miscible blend, while the material phase-separates with all other production techniques, such as solvent casting and spin coating. This effect has proven electrospinning the most effective production method, compared to solvent casting and spin coating, by preliminary thermal analysis conducted.

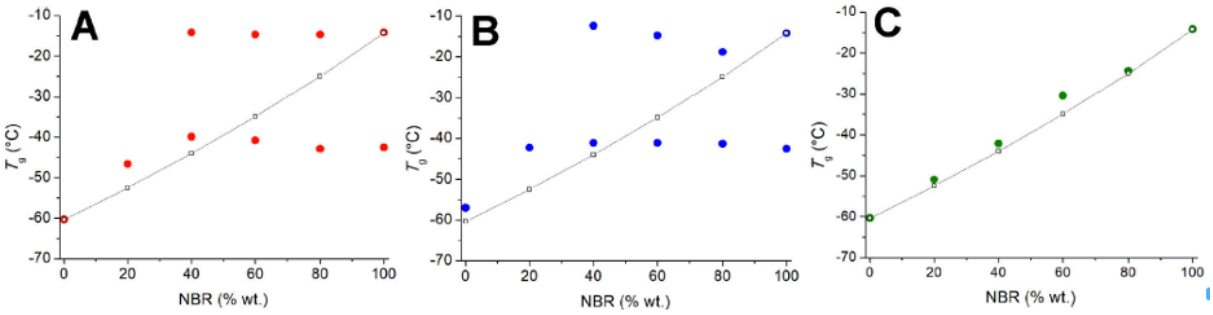

Figure 30: T_g as a function of NBR fraction (%wt) of solvent cast films (A), spin coating films (B), and nanofibrous mats (C). Solid dots: T_g from DSC analysis; white squares: T_g calculated by Fox equation (Equation 6)[82].

Figure 30 shows that films produced by solvent casting or spin coating undergo separate thermal events during DSC experiments, while electrospun membranes only exhibit one event. While the films, obtained from solvent casting, exhibit the T_g of both precursor polymers, the electrospun membrane shows only one thermal event that can be attributed to the combined T_g of the blend. The empirical Fox equation (Equation 6), listed below, shows the composition dependence of the blends T_g and has been used in Figure 30 to obtain the expected glass transition values for the comparison with the experimental data.

$$\frac{1}{T_g} = \frac{w_1}{T_{g1}} + \frac{w_2}{T_{g2}}$$

Equation 6: Fox equation, where w_1 and w_2 are the weight fractions and T_{g1} and T_{g2} are the glass transition temperatures (in Kelvin) of the polymer 1 and 2 respectively[82].

As mentioned above, the addition of PCL to NBR enables the production of stable nanofibers at room temperature. Also, the addition of NBR to PCL has a positive effect on the structural properties of the fibres. Henceforth, NBR acts as a nucleating agent in the compound, increasing the crystallinity of PCL at a given temperature. Figure 31 compares the expected melting enthalpy to measurements of the enthalpy of compounds with different fractions of PCL.

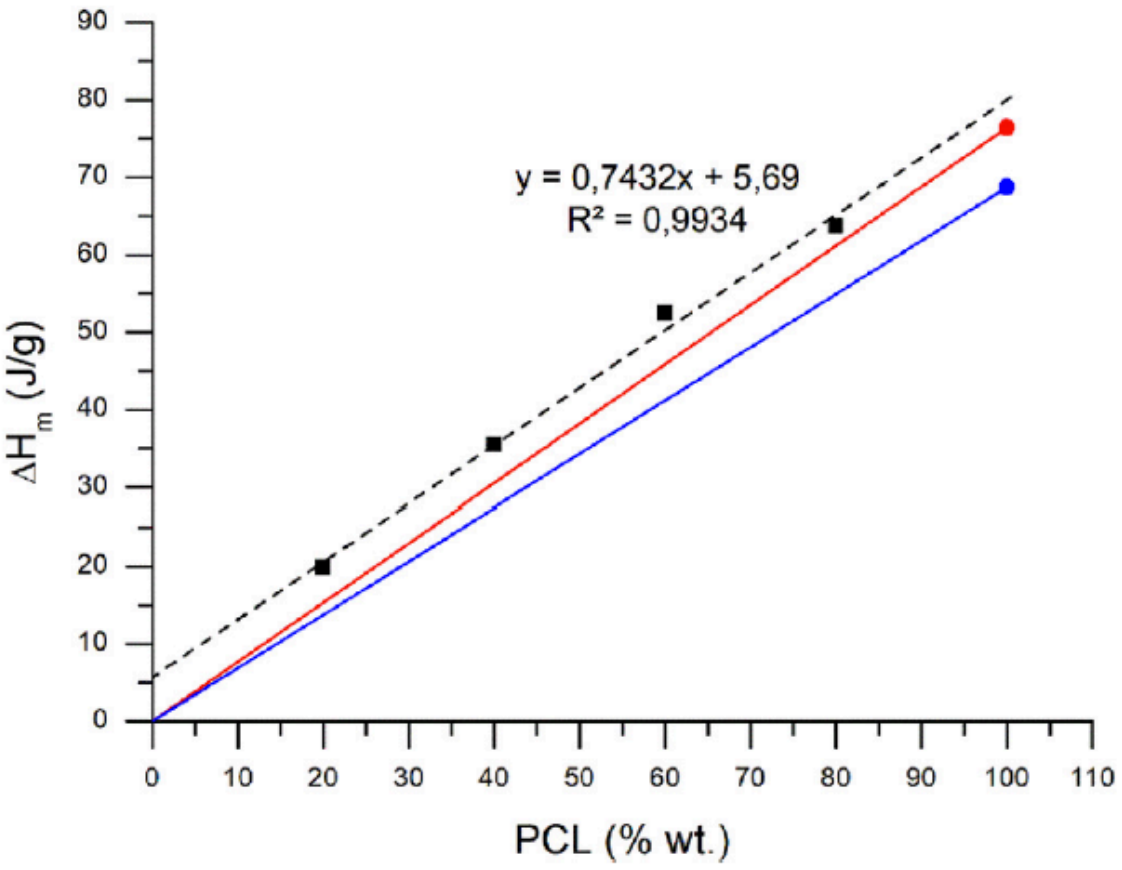

Figure 31: PCL melting enthalpy (ΔH_m) of NBR/PCL nanofibrous mats (black squares), PCL pellets (red dot) and PCL nanofibers (blue dot). Red and blue lines represent extrapolation of the enthalpy trend to 0% of PCL. The dashed black line is the linear regression for the NBR/PCL nanofibrous mat ΔH_m values[82].

Additional Wide-Angle X-Ray Scattering (WAXS) diffractograms show the refraction of the crystal phase in the polymer blend at 2 θ = 21,40° and 2θ = 23,70°.

The decrease of peak area in the diffractograms of membranes produced by electro-spinning, shown in Figure 32, corresponds to the build up of a PCL crystal phase.

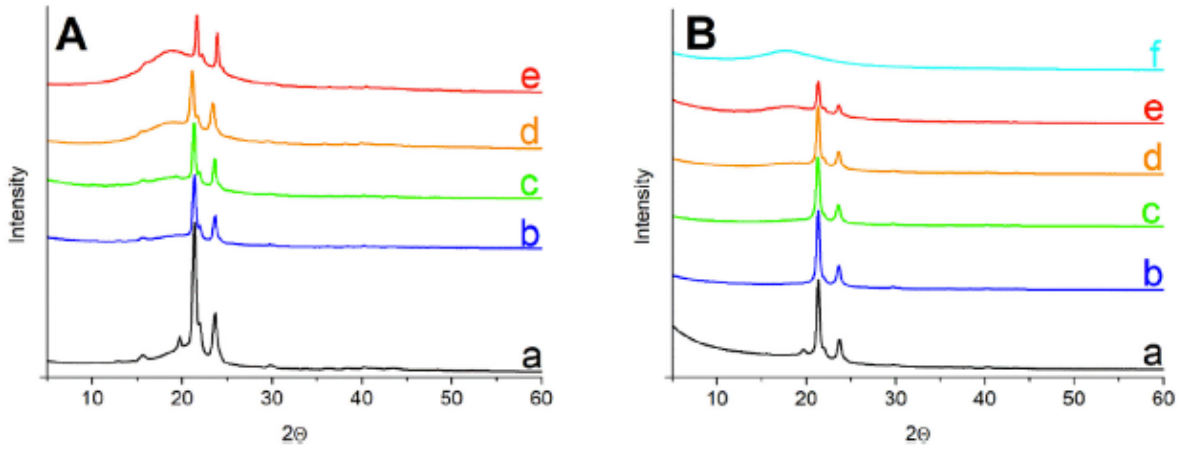

Figure 32: WAXS diffractograms of solvent cast films (A) and nanofibrous mats (B): a) PCL, b) 20/80, c) 40/60, d) 60/40, e) 80/20, f) NBR[82].

3.2 Production of nanofibers by electrospinning

The production of nanofibrous membranes, with thicknesses of 10, 20 and 40µm, was conducted by electrospinning and done in accordance to the description in chapter 1.5 as well as following the guidelines developed in preliminary studies by the research group. The machine, pictured in Figure 33, utilising a multineedle setup with a drum collector was used.

Figure 33: Multineedle electrospinning setup with drum collector.

The process was caried out under a hood to grant a stable environment for the nanofiber production. The specific parameters will follow in paragraph 5.2 of the experimental section. The drum collector was rotated at 50rpm to obtain membranes with randomly oriented nanofibers; a faster rotation of the collecting drum would instead contribute to preferential alignment of the forming fibres along the direction of rotation. The needle head was equipped with four needles simultaneously to increase productivity and it was translated continuously, in horizontal direction, to disperse the nanofibers over the whole area of the collector. The collector size, corresponding to a DIN A3 sheet, provides enough membrane material to produce enough samples of one thickness in one batch. In this way the behaviour of the final CFRP is expected to be independent from differing membrane conditions, like the diameter of fibres, their degree of orientation, actual thickness, etc.

Figure 34: Example of nanofibrous membrane on polyethylene coated paper, produced by electrospinning.

After the successful production of nanofibrous membranes in the three desired thicknesses, the membranes, as presented on the left in Figure 34, can be directly processed further. Due to the chemical and mechanical stability of the fibres, they maintain their shape and structure over a few weeks and can therefore be processed within a few days without any need of specific conservation. The right side of Figure 34 however, shows that the rubbery constitution of the fibres urges the membrane to lose contact to the collecting sheet of paper after multiple months of storage. This effect became apparent during the sudden disruption of the project due to the exceptional situation due to the COVID-19 pandemic, that required reprocessing of all the stored membranes that remained unattended during the duration of the lockdown.

3.3 Characterisation of nanofibers by scanning electron microscopy

Consecutively the obtained nanofibrous membranes have been examined with a SEM instrument, to evaluate their morphology. The following Figure 35 shows different magnifications of a 60/40 NBR/PCL membrane.

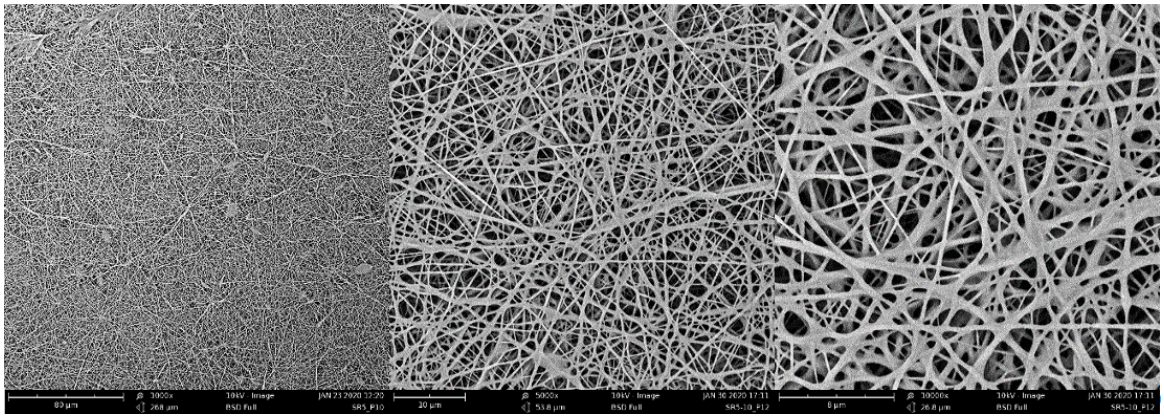

Figure 35: SEM images of 60/40 NBR/PCL blend nanofibrous mats with different magnifications (corresponding to the scale bars below the images).

The produced membranes are based on fibres with an average diameter of 259 ± 72nm and are randomly arranged. In conclusion, the membranes are of satisfying quality and can be used for further analysis.

3.4 Characterisation of nanofibers by Differential Scanning Calorimetry (DSC)

DSC measurements of fibres produced from the pure components and from the blend confirm their quality. As shown in Figure 36, the T_g of the blend lies in between the T_g of the single polymers, according to the Fox equation explained in chapter 3.1.

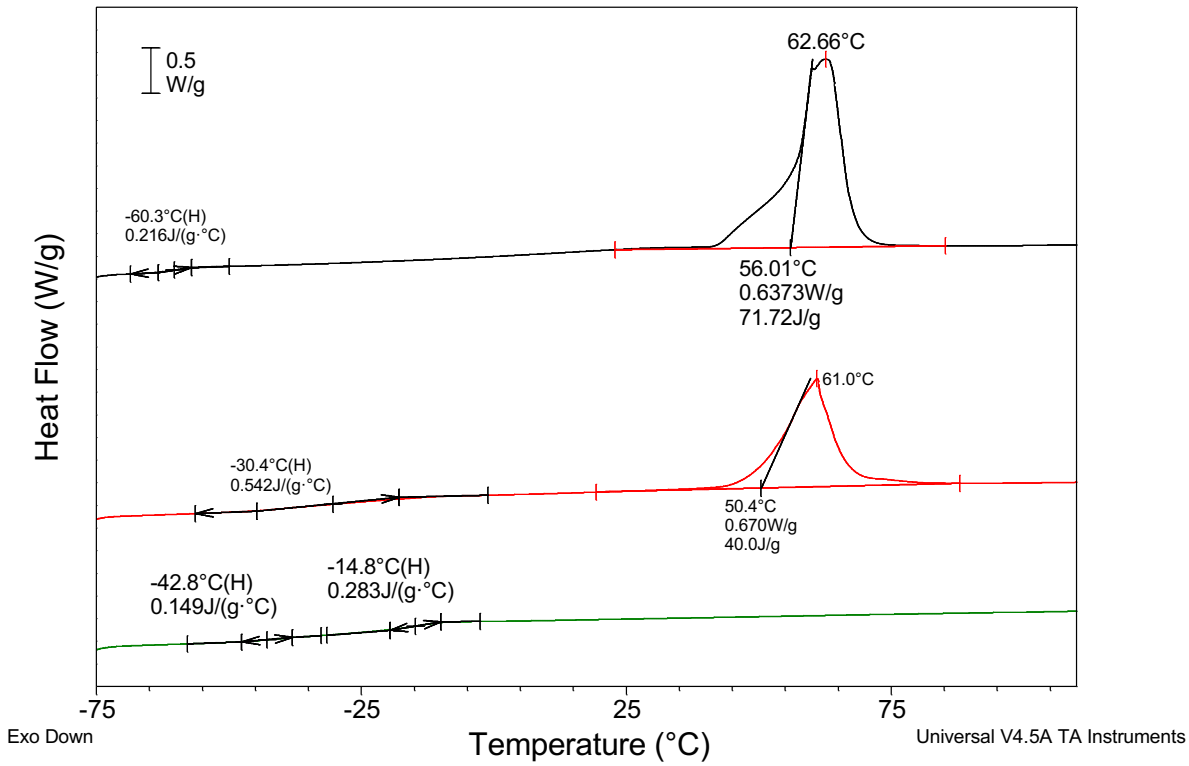

Figure 36: DSC results of pure PCL (black), NBR/PCL blend 60/40 (red), pure NBR (green).

The measurement affirmed the assumption that the two precursor polymers form a immiscible blend. According to the Fox equation (Equation 6) a successfully formed blend possesses a T_g value that lies between the T_g values of the precursors. In this case the theoretical value is $T_{g(NBR/PCL)theo.}$=-35,2°C, obtained by the application of the Fox equation to the values, reported in Figure 36, of the single polymeric precursors, $T_{g(NBR)}$=-14,8°C and $T_{g(PCL)}$=-60,3°C. The experimental value for $T_{g(NBR/PCL)exp.}$=-35,2°C is withing the tolerance and corresponds to a successful blend. Also the degree of crystallinity for the PCL fraction in the blend can be determined by comparison of the experimental melting enthalpy, reported in Figure 36, with that theoretically calculated

for a 100% crystalline polymer that the literature reports to be 139,5 J/g[88]. Indeed, while the measurement on pure PCL shows a degree of crystallinity around 51% upon electrospinning; when included in the blended nanofibers the degree of crystallinity of the sole PCL fraction is about 72%. Not considering the rubbery component as able to participate in the formation of the PCL like crystal phase. Such a huge value of crystallinity suggests that, beside a strong nucleating effect, some co-crystallisation might occur with a fraction of the NBR polymer within the crystal phase, that is in fact outgrowing the expected values on the basis of an unperturbed PCL behaviour. In the latter case, which constitutes a peculiar behaviour nonetheless, the expected melting enthalpy is estimated at 28,7J/g for the blend nanofibers. The solid like behaviour of the high crystal fraction enables the polymeric mixture to hold a stable fibrous morphology over time.

3.5 Composite production

During the next step, the obtained nanofibrous membranes as well as the provided carbon fibre prepregs were cut to size 80x40mm to suit the production of DMA convenient specimens (Figure 37).

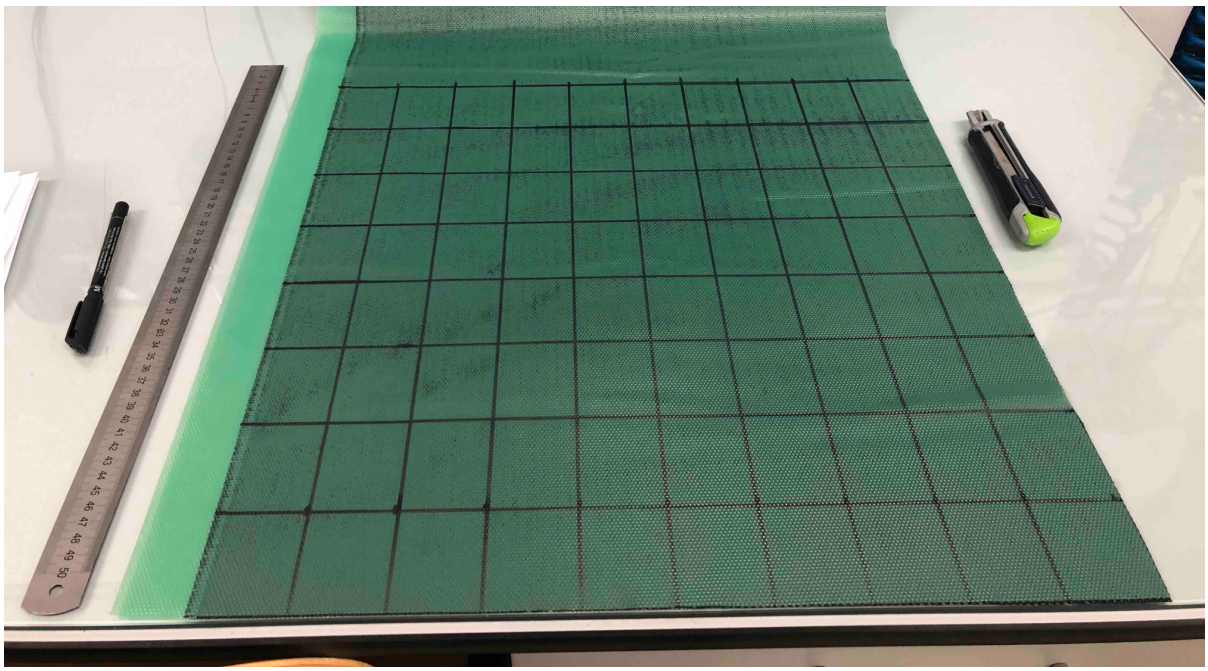

Figure 37: Preparation of Prepreg sheet before lamination.

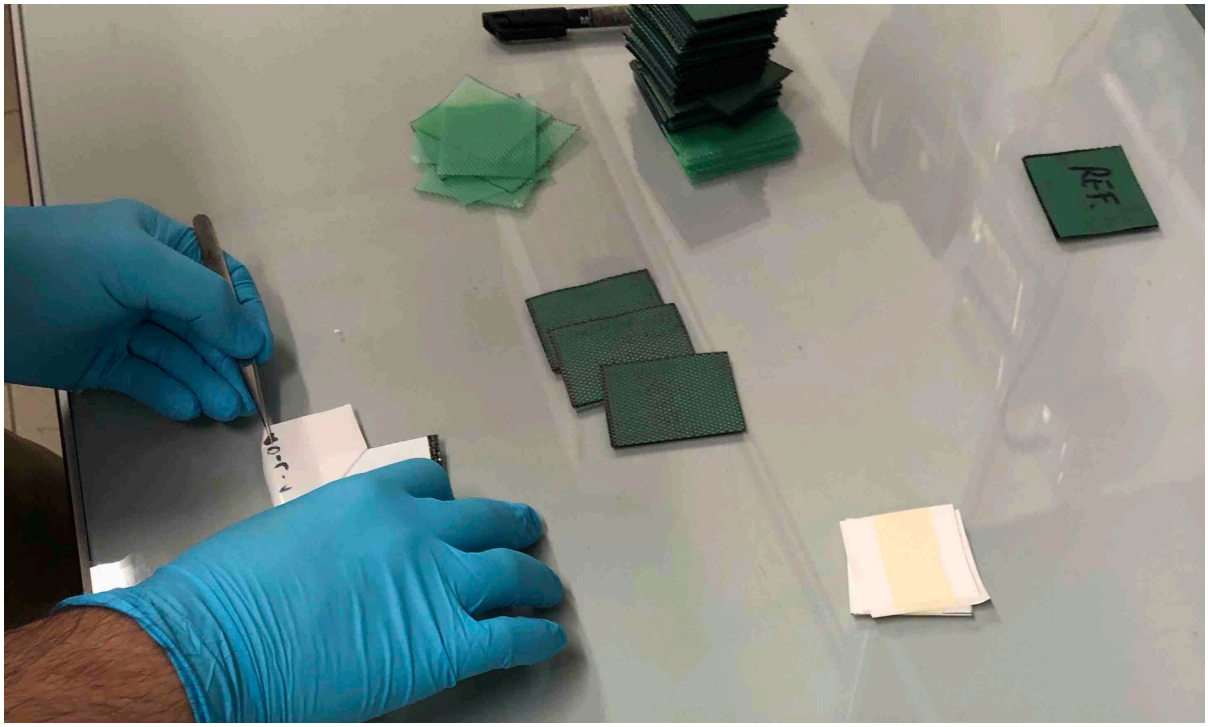

Figure 38: The process of layering of Prepregs and nanofibrous membranes.

Pictured in Figure 38, the prepregs and nanofibrous membranes are then layered up according to the stacking sequence displayed in Table 3.

Table 3: Stacking sequence for lamination phase. Prepreg layers (black), unmodified interfaces (white), modified interfaces (blue).

Reference	Sample A	Sample B	Sample C	Sample D	Sample E	Sample F

The stacking was carried out with membranes of thickness 10, 20 and 40µm separately, resulting in a total number of 19 samples (18 nanomodified + 1 unmodified). The reason to conduct the studies with three different membrane thicknesses is that the damping is expected to rise proportional to the modifications thickness. The stacking sequence was chosen to study the influence of the position and number of added nanofibrous membranes on the damping behaviour of the composite.

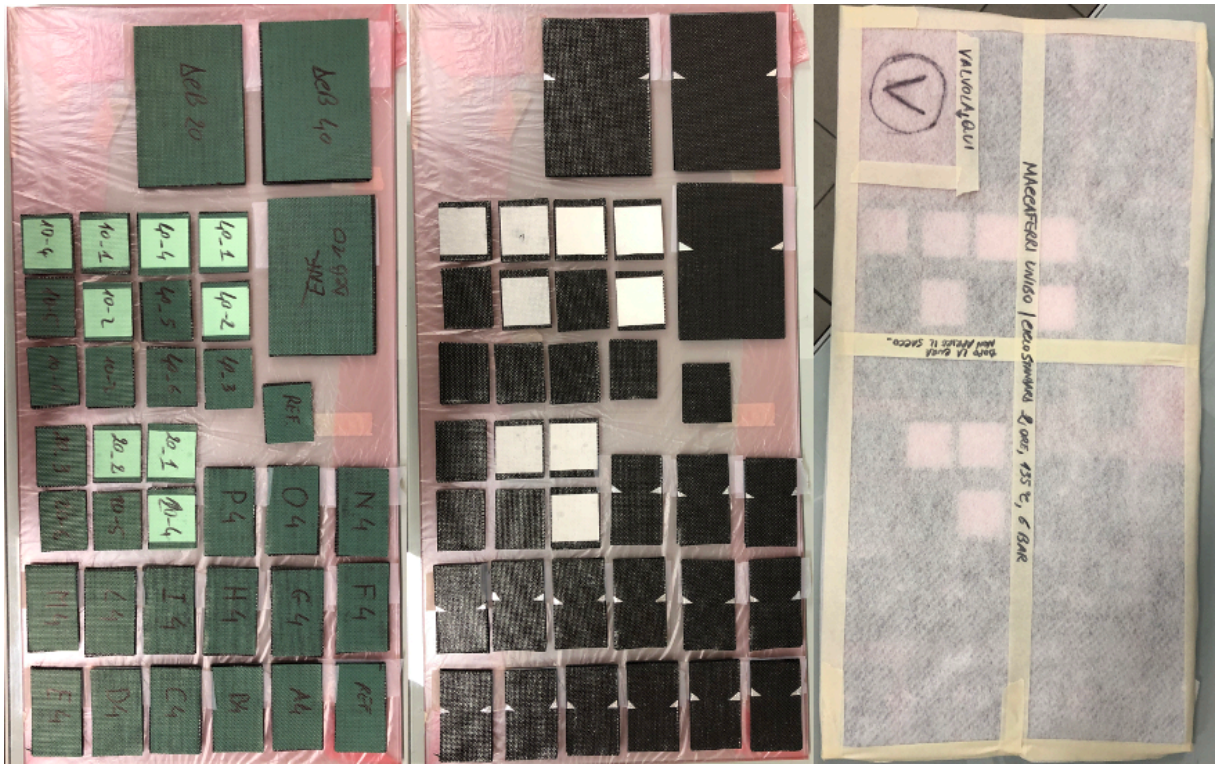

Figure 39: Preparation of laminate composites before curing.

Figure 39 documents the preparation of the produced laminates before they are subjected to an autoclave. Samples are placed on a glass surface and covered with a bag that is equipped with an added intermediate “breather” layer to aid the homogenous air removal during the application of a vacuum. The curing of the composites is done in two steps. In a first treatment, the plates were preheated under vacuum for two hours at 40°C to lower the resins viscosity, allowing it to creep and impregnate the nanofibrous membranes. During the second treatment, carried out at 135°C and 6bar for 1,5 hours, the nanofibers melt completely and blend together with the resin matrix. The resin matrix itself experiences an acceleration of the polymer crosslinking and therefore receives its final shape when the curing cycle is complete.

3.6 Dynamic Mechanical Analysis (DMA)

As established in the introduction, a polymers ability of viscoelastic deformation contributes highly to the materials ability to dampen vibrations and therefore avoid fatigue and delamination of the composite. DMA is an effective method to probe for the conditions in which a material is able to deform viscoelastically by evaluation of the tanδ values. As defined in paragraph 1.4.1, tanδ is also known as the damping factor. Therefore, the produced composite samples were tested individually by means of dynamic mechanical analysis to evaluate their damping behaviour, by qualitative comparison of their tanδ values as a function of temperature.

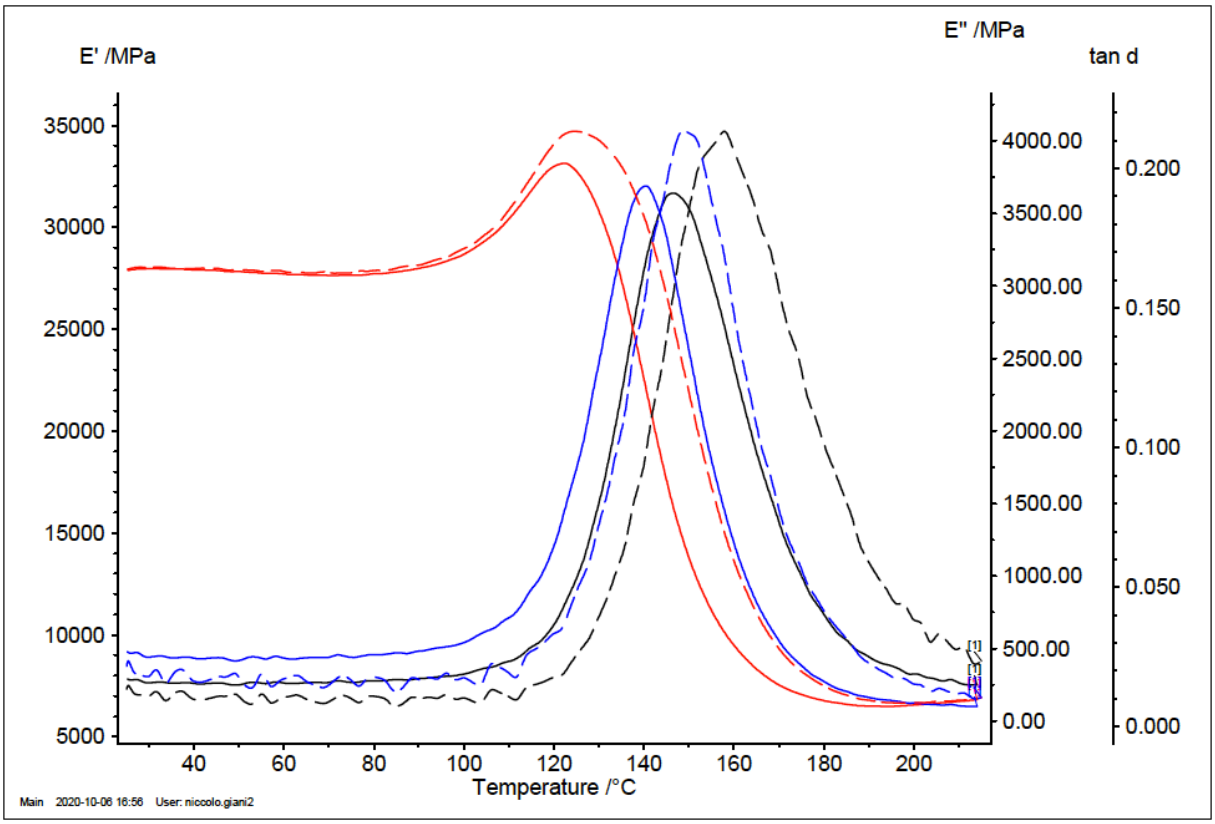

Figure 40: Result of DMA experiment on reference sample, carried out a 1Hz (uninterrupted lines) and 33,333Hz (dotted lines).

The reference sample, being an unmodified composite, was evaluated regarding the full information that can be obtained by the means of DMA. Figure 40 shows the results of a multiple frequency measurement. The uninterrupted line represents a measurement with the stress applied at 1Hz, while the dotted line was obtained with an applied stress at 33,333Hz. The two frequencies were chosen to check potential differences of behaviour in the analysed samples. Since the qualitative information doesn´t warry

between the measurements obtained by different frequency modes, the measurements at 33,333Hz were discarded and the further comments will be limited to the results obtained by experiments carried out at 1Hz.

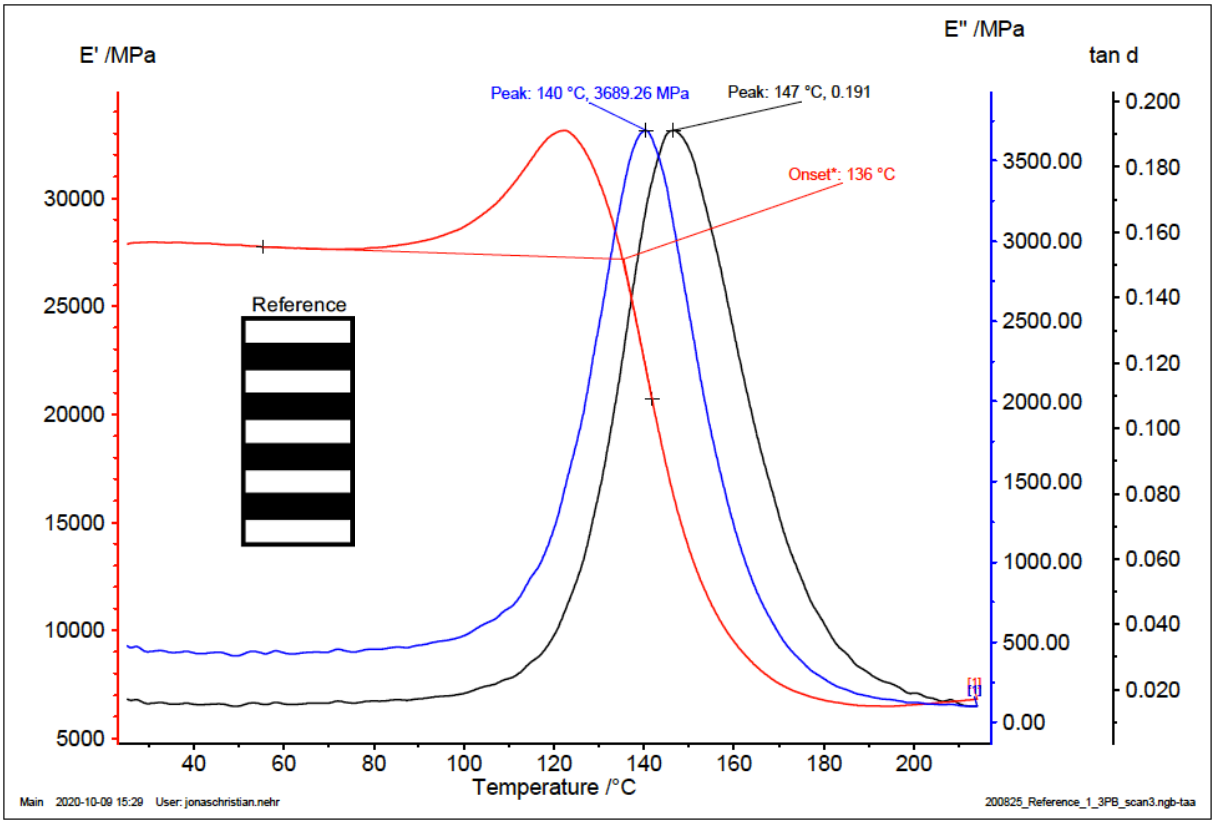

Figure 41: Result of DMA experiment on reference sample at 1Hz.

The conservative modulus (E`), the dissipative modulus (E´´) and the damping behaviour (tanδ) are depicted in Figure 41 to compare different methods to obtain the glass transition temperature of the composite from DMA measurements. While the T_g of a material and conclusions about its damping behaviour can be drawn from the onset of the E´ curve, from the maximum of E´´ and from the maximum of tanδ. While the E´ onset value, that points out the beginning of the cooperative motions that provide the overall polymer chain mobility, is the most conservative way to define the glass transition; the method utilising the tanδ curve is the most reliable for the present purpose, since it is not as sensible to disparities in the sample composition, like the alignment of reinforcement. The peak in the tanδ curve corresponds to the temperature region where the greatest part of the polymeric chains are able to move freely. For this reason and for the fact that the tanδ curve offers a good insight on the damping behaviour I have chosen to compare the following samples in the regard of the tanδ values.

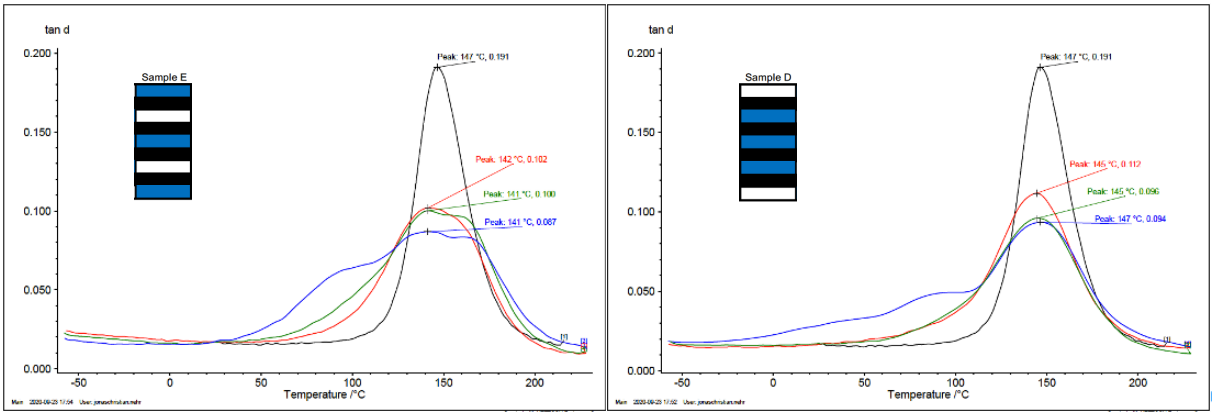

Figure 42: DMA results of sample E (left) and sample D (right); (Reference- black; modification thickness 10µm– red; modification thickness 20µm – green; modification thickness 40µm – blue).

Sample E and sample D, shown in Figure 42, while having the same number of modifications differ in their positioning. Sample E has modifications on the outer layers of the composite while in sample D the modification layers are bulked together in the centre of the sample. The DMA analysis shows that the damping behaviour in the bulk configuration in sample D is superior the intercepted stacking. The broadening of the tanδ curve corresponds to a widening of a relaxation temperature range in which the material has the capacity to dissipate energy and thus damp vibrations. The comparison to the unmodified reference sample shows that the broadening of tanδ is a result of the modification with nanofibrous membranes and increases with the membranes thickness. This phenomenon occurs mainly towards lower temperature, implying that the materials damping ability is extended down toward room temperature. While the increase in damping behaviour is a visible effect in sample E it appears as a weaker trend in sample D, simply because of the grouping nanomodifications.

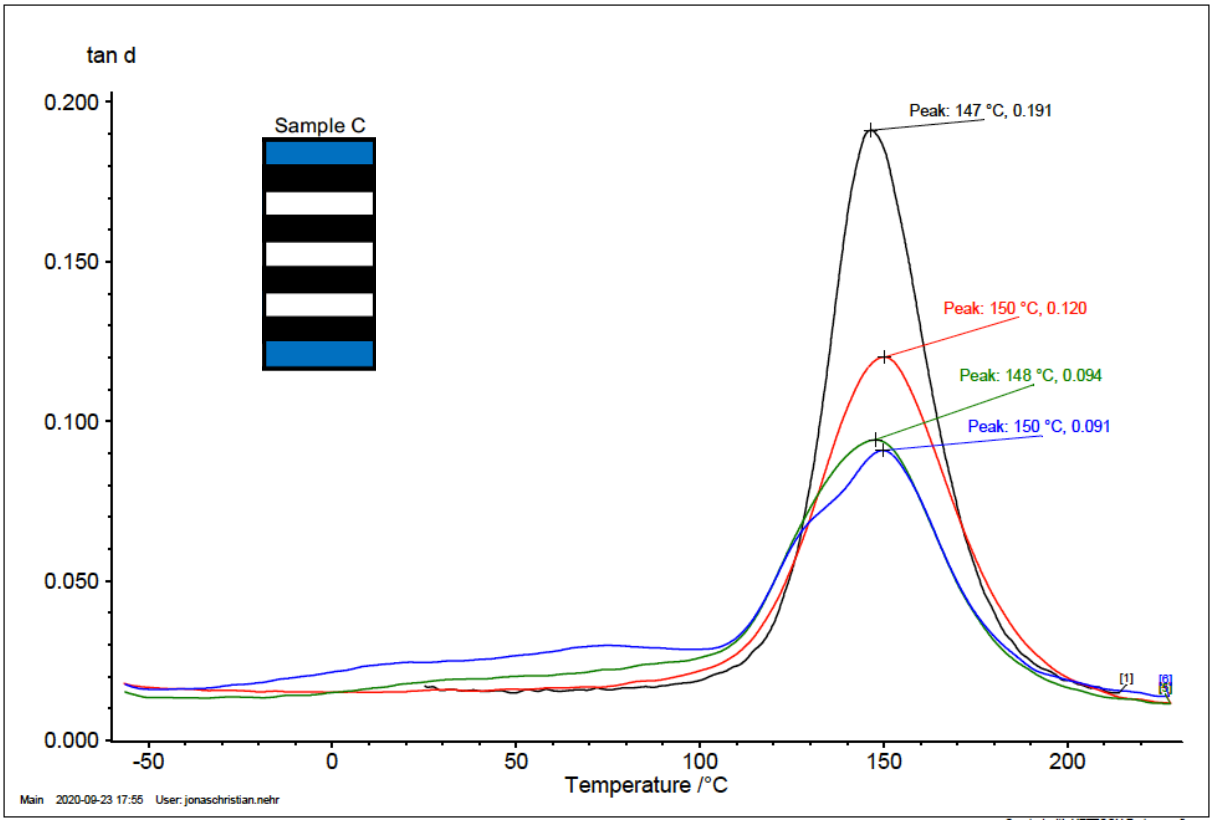

Figure 43: DMA result of sample C (Reference- black; modification thickness 10µm – red; modification thickness 20µm – green; modification thickness 40µm – blue).

The examination of sample C confirms the conclusion that a broadening of the damping temperature region can be accomplished by modification of lamination interfaces with nanofibrous modifications. Figure 43 shows that an increase in membrane thickness has a positive effect on the broadening of the tanδ curve, but since sample C inherited only modification at two terminal layers, that proves to be the least effective nanomodification, the visible effect is lower compared to previously discussed samples with more modifications.

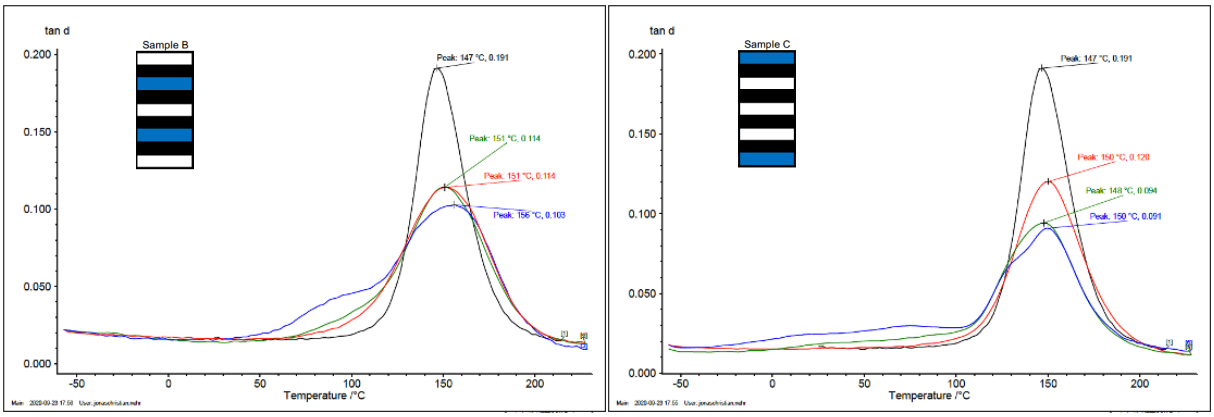

Figure 44: DMA results of sample B (left) and sample C (right); (Reference- black; modification thickness 10µm – red; modification thickness 20µm – green; modification thickness 40µm – blue).

Comparing the samples B and C, in Figure 44, both modified two times, gives another indication that the modification of the terminal layers of the laminates has a lower effect on the composites damping behaviour than the modification at interface layers.

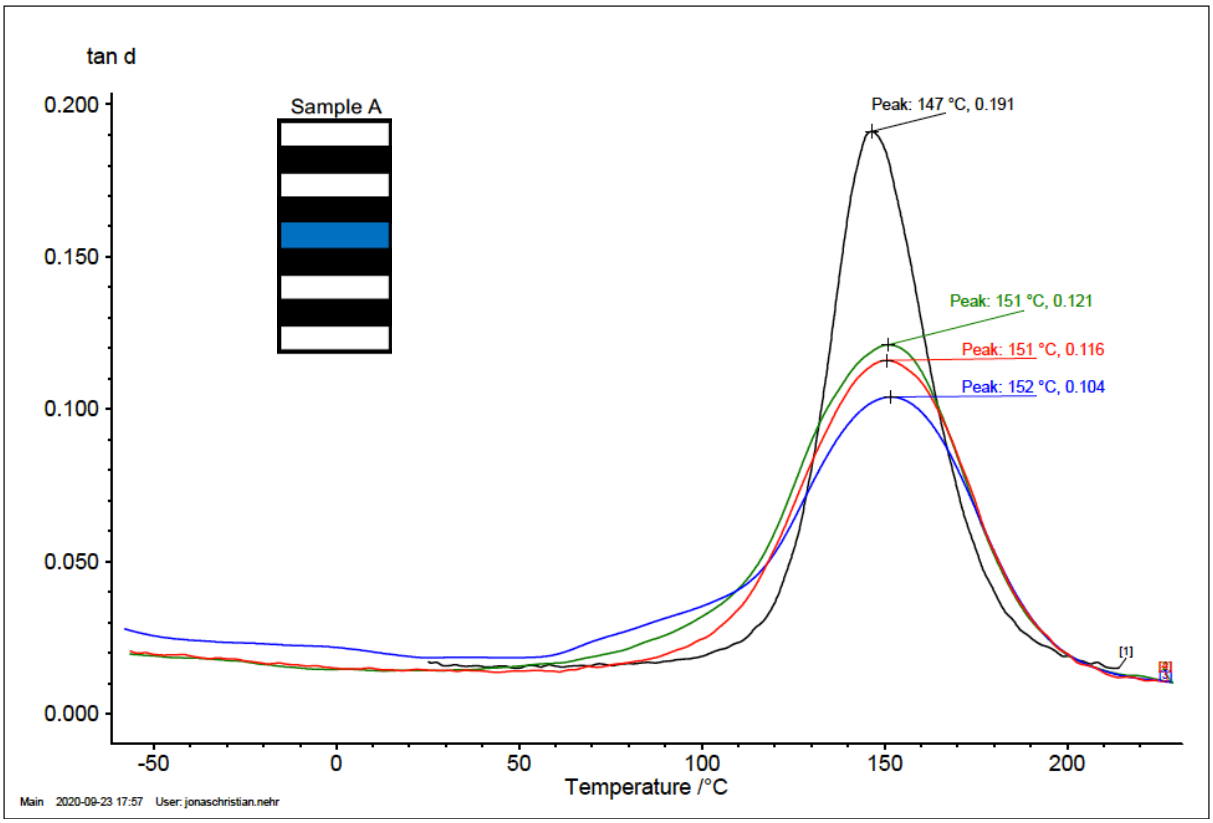

Figure 45: DMA results of sample A (Reference- black; modification thickness 10µm – red; modification thick-ness 20µm – green; modification thickness 40µm – blue).

Sample A in Figure 45, with only one modified layer shows the lowest effect on the damping behaviour at lower temperatures. The effect still rises with the thickness of the modification membrane. Both of these observations are in accordance with the formerly established expectations.

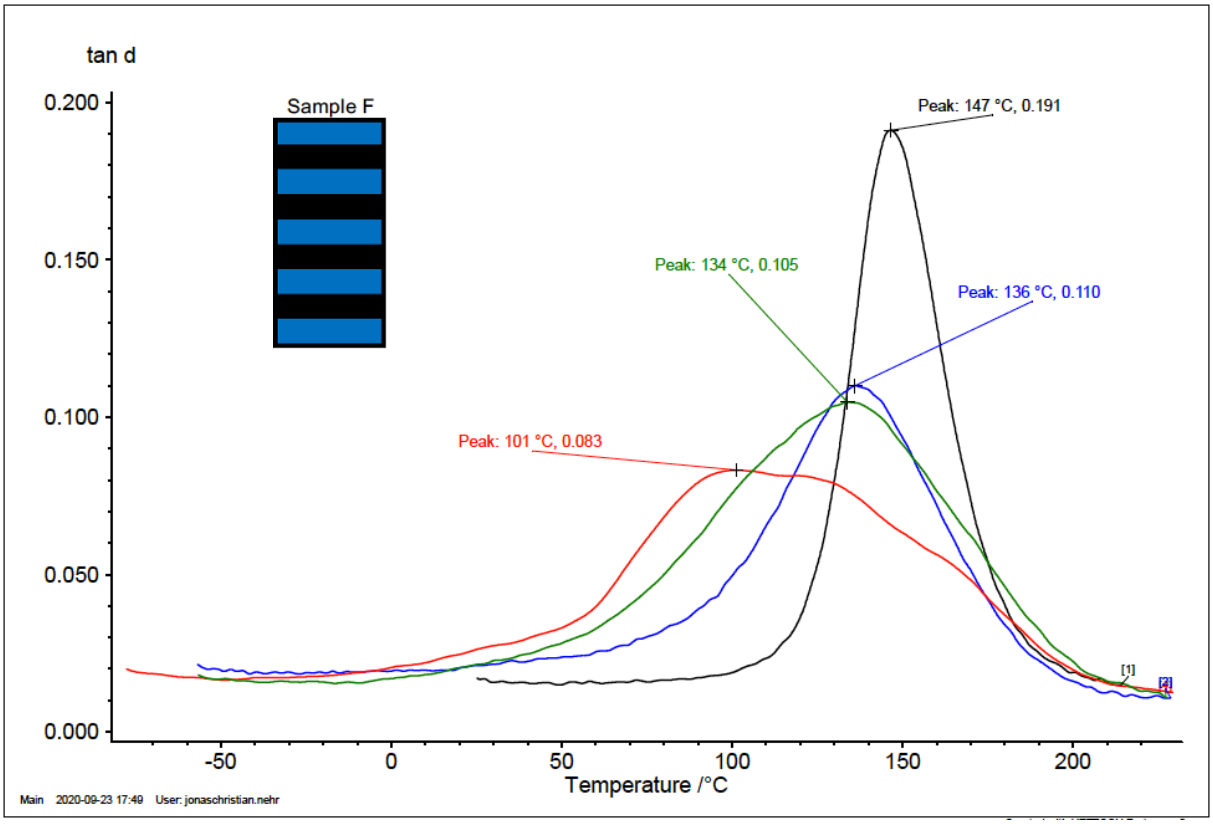

Figure 46: DMA results of sample F (Reference- black; modification thickness 10µm – red; modification thick-ness 20µm – green; modification thickness 40µm – blue).

While it can be expected, at this point, that the fully modified sample F exhibits the highest broadening of the tanδ curve, Figure 46 depicts an effect that exceeds the effect that the linear combination of tanδ values of, for example sample B and E suggests. Sample B and E have the same modifications together as sample F.

The earlier discussed set of data highlights that the position of the modifying layer plays a crucial role in the design of a damping component. Moreover, the evaluation of the modification position to attain the best performance might help to save material and to shape the final product. Additionally, the amount of material used can also be tailed via conveniently inserting nanomodifications in the most crucial regions of an object without the need to homogeneously modify the while bulk item.

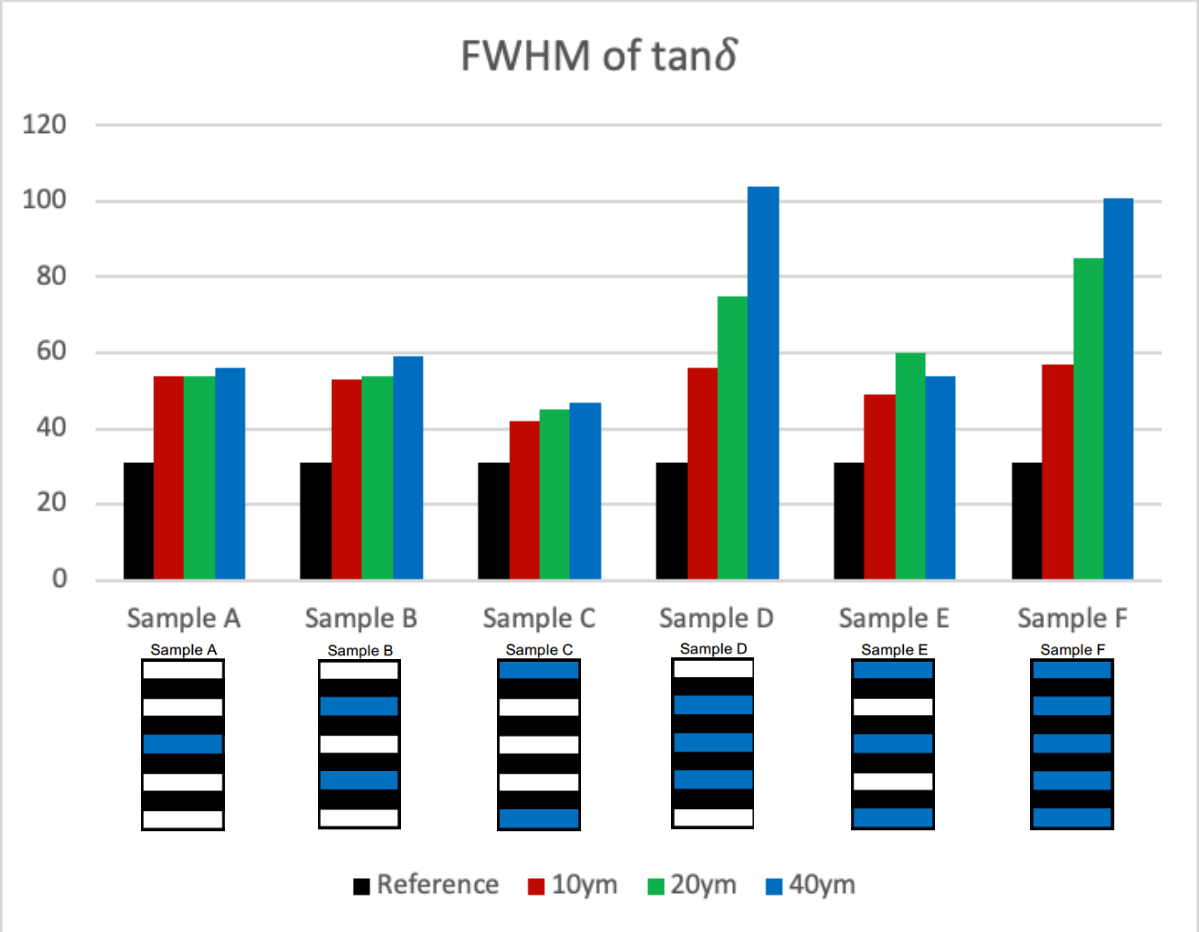

Figure 47: Full Width at Half Maximum (FWHM) of tanδ.

Finally, to provide an overall view on the potential effect of all the possible modifications, a comparison of the Full Width at Half Maximum (FWHM) of the tanδ curves, for all samples, is reported in Figure 47. This view at the data aids the assumption that the modification of a high number of interfaces with thick membranes widens the temperature range in which the material exhibits an improved damping capacity. As can be seen in Figure 47, the samples with the highest numbers of modified interfaces (D and F) offer the broadest temperature range. Sample D and F also testify to the importance of the thickness of the added membranes. While the samples with a low number of modifications demonstrate no strong dependence of the thickness, they indicate that also a low amount of modification widens the temperature region of damping.

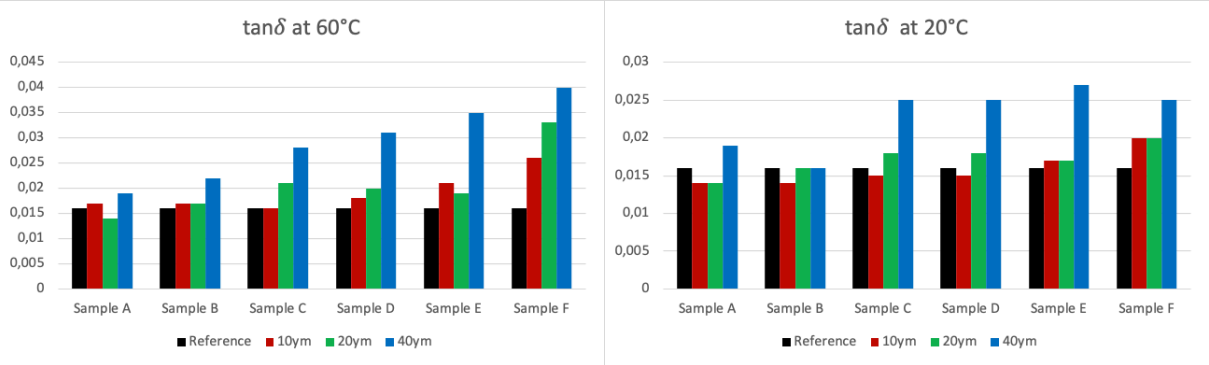

Figure 48: Tanδ values at 60°C and 20°C.

The tanδ values reported in Figure 48 show the dependence of the amount of modifications on the spread of the temperature range in which the damping can be improved. While the addition of 40µm membranes cause the damping effect to spread lower than 20°C even on samples with a low number of modifications; the addition of thinner membranes only manages to lower the temperature of effective damping until 60°C for highly modified samples, such as D and F. Only sample F, being modified at all interfaces, is able to spread the damping effect to the 20°C temperature region.

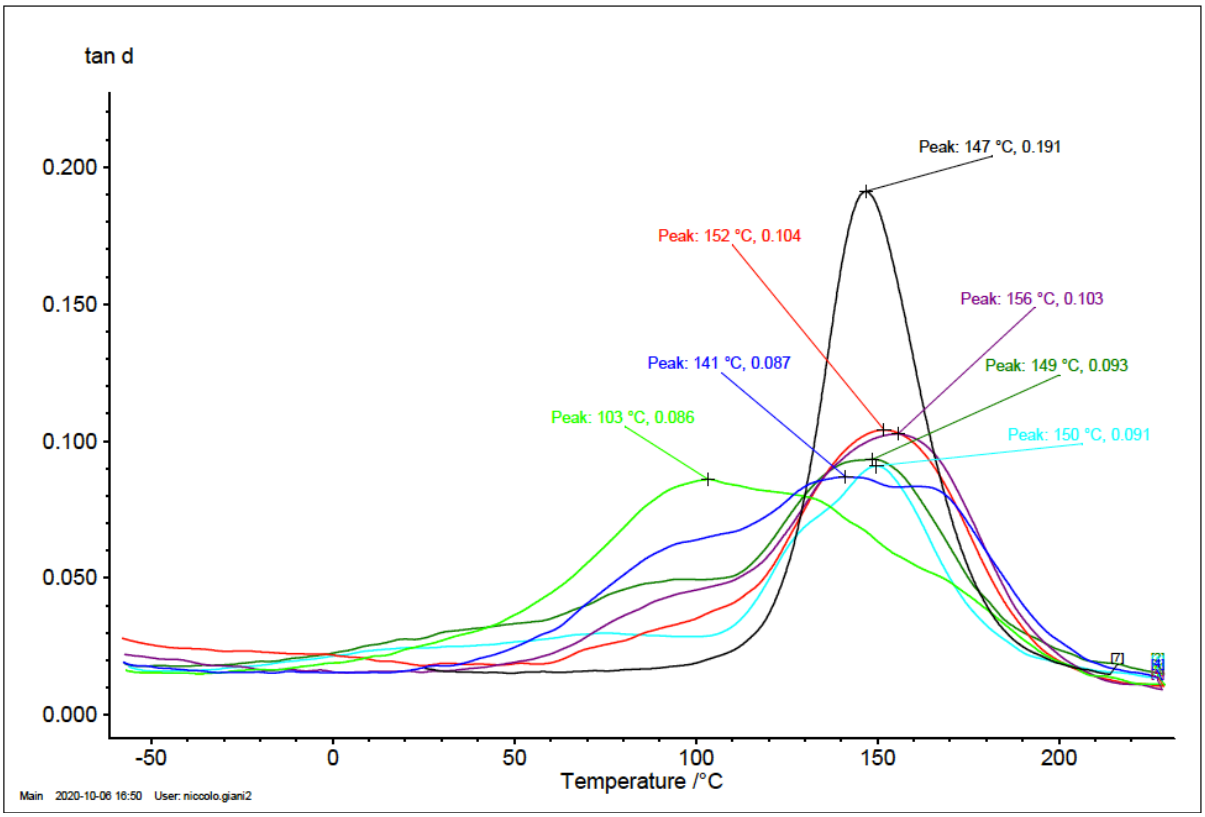

Figure 49: DMA results of all samples with modification thickness 40µm (Reference- black; sample A– red; sample B – green; sample C – blue; sample D – turquoise; sample E – purple; sample F – neon green).

Figure 49 stages the tanδ curves of all samples modified with a 40µm membranes and helps to visualise the effect of a growing number of modified interfaces on the damping behaviour.

4 Conclusion

In this thesis work, the effect of modifications with differing thickness, position and number of nanofibrous membranes in CFRP laminates with epoxy matrix was studied in regard to the damping behaviour. An improvement of the damping capacity is a promising approach to counteract on the intrinsic brittleness of stiff CFRP composites. This proposition rose from the insight of earlier research that damping can prohibit the formation of microcracks in the brittle epoxy matrix, leading to deterioration of the material and consequently preventing crack propagation in the matrix layer that would cause delamination. Apart from the positive effects on the lifetime of a product, damping also intercepts the propagation of vibration, which has a positive effect on the comfort of a product, by lowering ambient noise and mechanical vibrations.

The specific nanofibers used in this worked were made up by an immiscible blend of 60%wt NBR and 40%PCL, which has proven to be a combination capable of being easily processed, chemically stable, age resistant and provide improvement of laminate adhesion as well as the enhancement of damping in laminated CFRP composites. Additionally, NBR acts as a nucleating agent, favouring PCL crystallinity, effecting in structural stability of the fibres produced by electrospinning.

Electrospinning was established as a suitable method to produce structurally stable nanofibrous membranes from a solution of the precursor polymers NBR and PCL. The manufactured membranes showed no macroscopic defects and a SEM analysis confirmed the presence of randomly oriented fibres with diameters of 259 ± 72nm. Additional WAXS and DSC analysis were carried out to verify that the obtained fibres consist of an immiscible blend and, by evaluation of the degree crystallinity, to get an indirect indication of mechanical properties.

The membranes produced were incorporated, following different stacking sequences, in carbon fibre composites with an epoxy matrix, during the lamination phase. Nano-modified composites were obtained, after suitable pre-treatment and the subjection of a curing cycle in an autoclave.

Comparison of the differentially modified composites by their tanδ values, acquired by DMA measurements, suggests that the modification of interface laminate layers has a higher effect on the improvement of damping than the modification at terminal layers. The results also indicate the positive influence of a modification at all possible positions with thick membranes (within the range conducted in this series).

DMA analysis has unfolded that nanofibrous modification increases the damping capacity of CFRP drastically over a broad temperature range. It also suggests that all present laminate interfaces should be modified with thick membranes to maximise the temperature range of improved damping, at least in geometries sustaining high mechanical demand.

I personally suggest investigating the effect of thicker membranes, or the stacking of multiple thin membranes in one layer, further and also to apply the principle to asymmetrically modified composites.

5 Experimental Part

5.1 Materials

Carboxylated nitrile butadiene rubber (NBR) NIPOL 1072CGX, with 68%mol fraction of butadiene (Bu), 28%mol of acrylonitrile and 4%mol of methacrylic acid (MAA), was purchased from Zeon Chemicals and used without any pre-treatment.

Poly-(ε-caprolactone) (PCL), produced by Sigma-Aldrich with a molecular weight (Mw) between 70000-90000 Dalton was used without any pre-treatment.

Chloroform ($CHCl_3$), *N,N*-dimethylformamide (DMF) and *N,N*-dimethylacetamide (DMAc), produced by Sigma-Aldrich, were used without any further purification.

For the preparation of the polymeric solution, 10%wt NBR was dissolved in DMAc and 10%wt PCL was dissolved in a $CHCl_3$/DMF (1:1) solution under magnetic steering, in glass vials with airtight caps, at room temperature or mild heating. After the initial polymers were completely solubilized the precursor solution were blend together in the proportion of 60%wt NBR-solution and 40%wt PCL-solution to obtain the polymeric solution primed for the electrospinning process.

The prepreg (GG204P IMP503Z-HT), used for the CFRP production is made up from a plain weave carbon fabric (200 g/m^2) and an epoxy matrix. It was supplied by Angeloni s.r.l. (Venice, Italy)

5.2 Electrospinning

For the production of the nanofibrous mats a laboratory electrospinning unit with a multi-needle translating head and a rotating collector, manufactured by Spinbow was used. Four 5ml syringes were joined by Teflon tubing with needles of 55mm length and internal diameter of 0,84mm were used for the production of the nanofibrous membranes. The collector, rotating at 50 rpm was wrapped in polyethylene coated paper to ensure further processing of the obtained nanofibrous membranes.

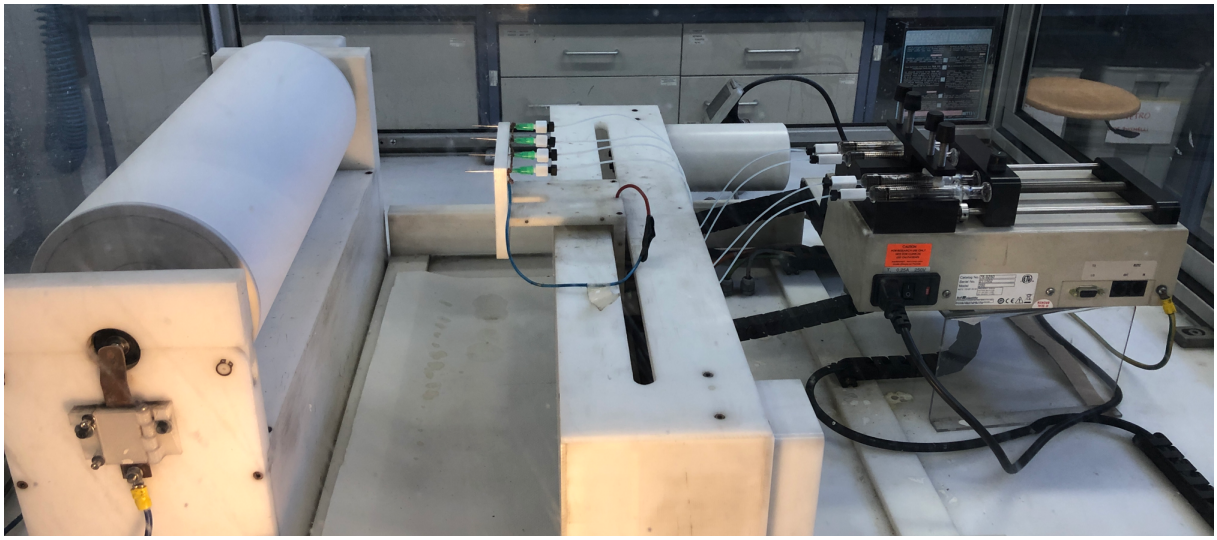

Figure 50: Electrospinning setup by Spinbow.

Figure 50 shows the full electrospinning setup, placed under a hood in order to minimise environmental influence and to ensure the safety of the laboratory. The process was carried out three times for different durations of time to obtain membranes of different thickness. The environmental conditions were stabilised under a hood at 23°C and a relative humidity of 20-22%. The distance from needle head to collector was kept at 13cm, while the flow rate of the polymeric solution was kept at 0,55ml/h and the electric potential between needles and collector constituted of 18,3 kV

5.3 Scanning electron microscopy (SEM)

The nanofibrous mats were analysed, regarding their morphology by Scanning Electron Microscopy (SEM) with a benchtop Phenom Pro X instrument from Zeiss. All analysed surfaces were coated with a gold/platinum alloy in order to create conductivity. The distribution of the fibres diameters was determined via manual measurement utilising the acquisition and image analysis software ImagePro Plus.

Differential Scanning Calorimetry (DSC) was conducted with a TA Instruments Q2000 DSC modulated apparatus equipped with a RCS cooling system. 5mg samples were heated, on non-hermetic aluminium foil pans, from -80°C to 120°C at 20°C/min in nitrogen atmosphere.

Wide-angle X-Ray Scattering (WAXS) was carried with a PANanalytical X´Pert PRO diffractometer equipped with an X´Celerator detector, for ultrafast data collection. A copper anode (K radiation: λ = 0.15418 nm, 40 kV, 40 mA) was used as a X-Ray source. The data was collected in a 2θ range from 2° to 60° through a ¼° divergence slit.

5.4 Composite production

Table 4: Stacking sequence for lamination phase. Prepreg layers (black), unmodified interfaces (white), modified interfaces (blue).

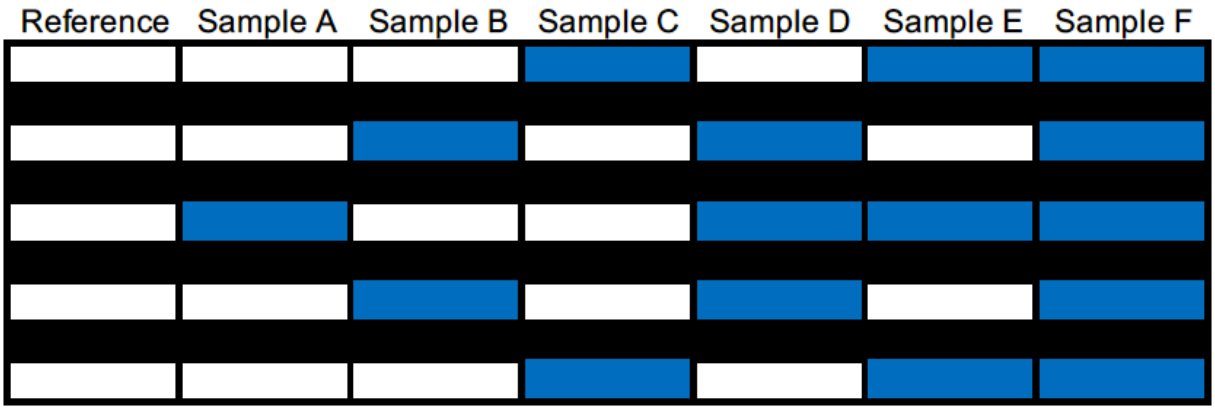

Composite samples were stacked up manually following the stacking sequences described in Table 4. The plates were cured in an autoclave for 1h and 30min at 135°C, 6bar, after having carried out a pre-treatment under vacuum for two hours at 40°C.

5.5 DMA

After the successful execution of the curing cycle the samples were cut to size 40x80mm. Dynamic Mechanical Analysis (DMA) was carried out, on all 19 composite samples, with a DMA 242 E Artemis instrument by Netzsch. The analysis was conducted with a 20mm three-point bending geometry in a temperature ramp from -80°C to 230°C with a heating rate of 3°C per minute, stress was applied simultaneously at 1Hz frequency with an 20µm amplitude, a maximum dynamic force of 8N and a static force/dynamic force ratio of 1,5.

6 References

1. McElhinney D.M., Kitchenside A.W. & Rowland K.A. The Use of Carbon Fibre Reinforced Plastics: A review of the progress made in the practical application of CFRP to conventional commercial aircraft structures. *Aircr. Eng. Aerosp. Technol.* **41**, 22–25 (1969).

2. *Handbuch Eurocode 4 - Verbundbau (Stahl und Beton): Band 2: Brücken*. (Beuth).

3. V, D. I. N. *Farbmittel 1: Pigmente, Füllstoffe, Farbstoffe DIN-Normen*. (Beuth Verlag GmbH, 2012).

4. Anaee, R. A. M. & Abdulmajeed, M. H. Tribocorrosion. (2016) doi:10.5772/63657.

5. Goris, A. *Stahlbetonbau-Praxis nach Eurocode 2 - Band 1*. (Bauwerk Verlag GmbH, 2010).

6. Mallick, P. *Fiber-Reinforced Composites: Materials, Manufacturing, And Design*. *Fiber-Reinforced Composites: Materials, Manufacturing, and Design, Third Edition* vol. 2 (2007).

7. Ning, F., Cong, W., Wei, J., Wang, S. & Zhang, M. Additive Manufacturing of CFRP Composites Using Fused Deposition Modeling: Effects of Carbon Fiber Content and Length. in *MSEC2015* (2015). doi:10.1115/MSEC2015-9436.

8. Huang, Y., Jin, K.-K. & ha, S. Effects of Fiber Arrangement on Mechanical Behavior of Unidirectional Composites. *J. Compos. Mater. - J COMPOS MATER* **42**, 1851–1871 (2008).

9. Singh, M. Latest Advancements In Carbon Based Fiber, A Review. in (2017).

10. Soutis, C. Fibre reinforced composites in aircraft construction. *Prog. Aerosp. Sci.* **41**, 143–151 (2005).

11. Huang, X. Fabrication and Properties of Carbon Fibers. *Materials* **2**, 2369–2403 (2009).

12. BlackWing Aircraft Reinforced by TeXtreme Wins Red Dot Design Award. *NetComposites* https://netcomposites.com/news/blackwing-aircraft-reinforced-by-textreme-wins-red-dot-design-award/.

13. McLaren 12C - Innovation | McLaren Automotive. https://cars.mclaren.com/us-en/legacy/12c/innovation.

14. Benedict, T. EB18: Carbon-Ti carbon fiber chainrings for Dura-Ace & SRM, CarbonSteel brake rotors. *Bikerumor* https://bikerumor.com/2018/07/19/eb18-carbon-ti-carbon-fiber-chainrings-for-dura-ace-srm-carbonsteel-brake-rotors/ (2018).

15. One shot socket. *Blatchford - Mobility Made Possible* https://www.blatchford.co.uk/products/one-shot-socket/.

16. Kubba, S. Chapter 9 - Impact of Energy and Atmosphere. in *Handbook of Green Building Design and Construction* (ed. Kubba, S.) 385–492 (Butterworth-Heinemann, 2012). doi:10.1016/B978-0-12-385128-4.00009-3.

17. Johnson, D. J. Structure and Properties of Carbon Fibres. in *Carbon Fibers Filaments and Composites* (eds. Figueiredo, J. L., Bernardo, C. A., Baker, R. T. K. & Hüttinger, K. J.) 119–146 (Springer Netherlands, 1990). doi:10.1007/978-94-015-6847-0_5.

18. Frank, E., Steudle, L. M., Ingildeev, D., Spörl, J. M. & Buchmeiser, M. R. Carbon Fibers: Precursor Systems, Processing, Structure, and Properties. *Angew. Chem. Int. Ed.* **53**, 5262–5298 (2014).

19. Bhatt, P. & Goe, A. Carbon Fibres: Production, Properties and Potential Use. *Mater. Sci. Res. India* **14**, 52–57 (2017).

20. Frank, E., Ingildeev, D. & Buchmeiser, M. R. High-performance PAN-based carbon fibers and their performance requirements. in *Structure and Properties of High-Performance Fibers* (ed. Bhat, G.) 7–30 (Woodhead Publishing, 2017). doi:10.1016/B978-0-08-100550-7.00002-4.

21. Frank, E., Hermanutz, F. & Buchmeiser, M. R. Carbon Fibers: Precursors, Manufacturing, and Properties. *Macromol. Mater. Eng.* **297**, 493–501 (2012).

22. Prof. Greene, J. Reinforcements. (2011).

23. Wonderly, C., Grenestedt, J., Fernlund, G. & Cěpus, E. Comparison of mechanical properties of glass fiber/vinyl ester and carbon fiber/vinyl ester composites. *Compos. Part B Eng.* **36**, 417–426 (2005).

24. Russo, S. Incremento della tenacità a frattura interlaminare di Modo I e II in CFRP mediante l'uso di nanofibre polimeriche ottenute per elettrofilatura. (University of Bologna).

25. Park, S.-J. *Carbon Fibers*. (Springer Netherlands, 2015). doi:10.1007/978-94-017-9478-7.

26. McCrum, C. B. *Principles of polymer engineering*. vol. 21 (John Wiley & Sons, 2009).

27. aurelie08. Disadvantages of carbon fiber. *Solar Car monocoque* https://solarcarmonocoque.wordpress.com/2014/03/23/disadvantages-of-carbon-fiber/ (2014).

28. Helfen, T. B., Venkat, R. S., Rabe, U., Hirsekorn, S. & Boller, C. Characterisation of

CFRP Through Enhanced Ultrasonic Testing Methods. *Appl. Compos. Mater.* **19**, 913–919 (2012).

29. Melentiev, R., Priarone, P. C., Robiglio, M. & Settineri, L. Effects of Tool Geometry and Process Parameters on Delamination in CFRP Drilling: An Overview. *3rd CIRP Conf. Surf. Integr.* **45**, 31–34 (2016).

30. Li, Y., Li, Q. & Ma, H. The voids formation mechanisms and their effects on the mechanical properties of flax fiber reinforced epoxy composites. *Compos. Part Appl. Sci. Manuf.* **72**, 40–48 (2015).

31. Perner, M., Algermissen, S., Keimer, R. & Monner, H. P. Avoiding defects in manufacturing processes: A review for automated CFRP production. *Robot. Comput.-Integr. Manuf.* **38**, 82–92 (2016).

32. Haeger, A. *et al.* Interaction between laminate quality, drilling-induced delamination and mechanical properties in machining of carbon fibre reinforced plastic (CFRP). *Mater. Werkst.* **47**, 997–1014 (2016).

33. Arai, M. *et al.* Mixed modes interlaminar fracture toughness of cfrp laminates toughened with CNF interlayer. *Acta Mech. Solida Sin.* **25**, 321–330 (2012).

34. Brugo, T. & Palazzetti, R. The effect of thickness of Nylon 6,6 nanofibrous mat on Modes I–II fracture mechanics of UD and woven composite laminates. *Compos. Struct.* **154**, 172–178 (2016).

35. SCHULTE, K. & STINCHCOMB, W. W. Chapter 8 - Damage Mechanisms - Including Edge Effects - in Carbon Fibre-reinforced Composite Materials. in *Composite Materials Series* (ed. Friedrich, K.) vol. 6 273–324 (Elsevier, 1989).

36. Marjanović, M., Meschke, G. & Vuksanović, D. A finite element model for propagating delamination in laminated composite plates based on the Virtual Crack Closure method. *Compos. Struct.* **150**, 8–19 (2016).

37. Pedemonte, E. *Fondamenti di struttura, proprietà e tecnologia dei polimeri*. vol. 4 (Nuova Cultura, 2004).

38. Yun, N. G., Won, Y. G. & Kim, S. C. Toughening of carbon fiber/epoxy composite by inserting polysulfone film to form morphology spectrum. *Polymer* **45**, 6953–6958 (2004).

39. Matsuda, S. *et al.* Effect of ionomer thickness on mode I interlaminar fracture toughness for ionomer toughened CFRP. *Compos. Part Appl. Sci. Manuf.* **30**, 1311–1319 (1999).

40. Zhang, J., Yang, T., Lin, T. & Wang, C. H. Phase morphology of nanofibre interlayers: Critical factor for toughening carbon/epoxy composites. *Compos. Sci. Technol.* **72**, 256–262 (2012).

41. Dzenis, Y. & Reneker, D. Delamination Resistant Composites Prepared by Small Diameter Fiber Reinforcement at Ply Interfaces. *Mech. Mater. Eng. Fac. Publ.* (2001).

42. Li, G. *et al.* Inhomogeneous toughening of carbon fiber/epoxy composite using electrospun polysulfone nanofibrous membranes by in situ phase separation. *Compos. Sci. Technol.* **68**, 987–994 (2008).

43. Brugo, T. *et al.* Study on Mode I fatigue behaviour of Nylon 6,6 nanoreinforced CFRP laminates. *Compos. Struct.* **164**, 51–57 (2017).

44. Beards, C. F. Chapter 5 - Damping in structures. in *Structural Vibration* (ed. Beards, C. F.) 157–204 (Butterworth-Heinemann, 1996). doi:10.1016/B978-034064580-2/50007-7.

45. Mucchi, E. Experimental evaluation of modal damping in automotive components with different constraint conditions. *Meccanica* **47**, 1035–1041 (2012).

46. Assarar, M., Zouari, W., Ayad, R., Kebir, H. & Berthelot, J.-M. Improving the damping properties of carbon fibre reinforced composites by interleaving flax and viscoelastic layers. *Compos. Part B Eng.* **152**, 248–255 (2018).

47. Bangarubabu, P., Kumar, K. & Krishna, Y. Damping Effect of Viscoelastic Materials on Sandwich Beams. in.

48. Napolitano, K. L., Grippo, W., Kosmatka, J. B. & Johnson, C. D. A comparison of two cocured damped composite torsion shafts. *Compos. Struct.* **43**, 115–125 (1998).

49. Epaarachchi, J. A. 17 - The effect of viscoelasticity on fatigue behaviour of polymer matrix composites. in *Creep and Fatigue in Polymer Matrix Composites* (ed. Guedes, R. M.) 492–513 (Woodhead Publishing, 2011). doi:10.1533/9780857090430.3.492.

50. Nielsen, L. F. Viscoelastic Composites. in *Composite Materials: Properties as Influenced by Phase Geometry* (ed. Nielsen, L. F.) 199–220 (Springer, 2005). doi:10.1007/978-3-540-27680-7_15.

51. Mazzocchetti, L. *et al.* Poly-m-aramid electrospun nanofibrous mats as high-performance flame retardants for carbon fiber reinforced composites. *Compos. Part B Eng.* **145**, 252–260 (2018).

52. Anton, F. Process and apparatus for preparing artificial threads. (1934).

53. Taylor, G. I. Disintegration of water drops in an electric field. *Proc. R. Soc. Lond. Ser. Math. Phys. Sci.* **280**, 383–397 (1964).

54. Quek, S. Y., Hadi, J. & Tanambell, H. Application of Electrospinning as Bioactive Delivery System. in *Encyclopedia of Food Chemistry* (eds. Melton, L., Shahidi, F. & Varelis, P.) 145–149 (Academic Press, 2019). doi:10.1016/B978-0-08-100596-5.22464-5.

55. Basson, N. Free volume of electrospun organic-inorganic copolymers. (2014).

56. Bhardwaj, N. & Kundu, S. C. Electrospinning: A fascinating fiber fabrication technique. *Biotechnol. Adv.* **28**, 325–347 (2010).

57. Sill, T. J. & von Recum, H. A. Electrospinning: Applications in drug delivery and tissue engineering. *Biomaterials* **29**, 1989–2006 (2008).

58. Lim, L.-T., Mendes, A. C. & Chronakis, I. S. Chapter Five - Electrospinning and electrospraying technologies for food applications. in *Advances in Food and Nutrition Research* (eds. Lim, L.-T. & Rogers, M.) vol. 88 167–234 (Academic Press, 2019).

59. Lee, K.-H., Kim, hy, Bang, H. J., Jung, Y. H. & Lee, S. The change of bead morphology formed on electrospun polystyrene fibers. *Polymer* **44**, 4029–4034 (2003).

60. Deitzel, J. M., Kleinmeyer, J., Harris, D. & Beck Tan, N. C. The effect of processing variables on the morphology of electrospun nanofibers and textiles. *Polymer* **42**, 261–272 (2001).

61. Campeti, J. Modifica strutturale di CFRP laminati mediante integrazione di tessuti nanofibrosi. (University of Bologna).

62. Supaphol, P., Mit-uppatham, C. & Nithitanakul, M. Ultrafine Electrospun Polyamide-6 Fibers: Effects of Solvent System and Emitting Electrode Polarity on Morphology and Average Fiber Diameter. *Macromol. Mater. Eng.* **290**, 933–942 (2005).

63. Yuan, X., Zhang, Y., Dong, C. & Sheng, J. Morphology of ultrafine polysulfone fibers prepared by electrospinning. *Polym. Int. - POLYM INT* **53**, 1704–1710 (2004).

64. Reneker, D. H. & Chun, I. Nanometre diameter fibres of polymer, produced by electrospinning. *Nanotechnology* **7**, 216–223 (1996).

65. Zhang, C., Yuan, X., Wu, L., Han, Y. & Sheng, J. Study on morphology of electrospun poly(vinyl alcohol) mats. *Eur. Polym. J.* **41**, 423–432 (2005).

66. Egerton, R. F. *Physical Principles of Electron Microscopy: An Introduction to TEM, SEM, and AEM*. (Springer US, 2005). doi:10.1007/b136495.

67. Reimer, L. Scanning Electron Microscopy: Physics of Image Formation and Microanalysis, Second Edition. *Meas. Sci. Technol.* **11**, 1826–1826 (2000).

68. Suzuki, E. High-resolution scanning electron microscopy of immunogold-labelled cells by the use of thin plasma coating of osmium. *J. Microsc.* **208**, 153–157 (2002).

69. Demarest, S. J. & Frasca, V. Chapter 11 - Differential scanning calorimetry in the biopharmaceutical sciences. in *Biophysical Characterization of Proteins in Developing Biopharmaceuticals (Second Edition)* (eds. Houde, D. J. & Berkowitz, S. A.) 311–332 (Elsevier, 2020). doi:10.1016/B978-0-444-64173-1.00011-1.

70. Rudin, A. & Choi, P. *The Elements of Polymer Science and Engineering*. (Academic Press, 2012).

71. Pascault, J.-P., Sautereau, H., Verdu, J. & Williams, R. J. J. *Thermosetting Polymers*. (CRC Press, 2002).

72. Menard, K. P. *Dynamic Mechanical Analysis : A Practical Introduction, Second Edition*. (CRC Press, 2008). doi:10.1201/9781420053135.

73. Dynamic Mechanical Analysis (DMA) A Beginner's Guide. 23.

74. Yazdi, M. H. & Lee-Sullivan, P. Determination of dual glass transition temperatures of a PC/ABS blend using two TMA modes. *J. Therm. Anal. Calorim.* **96**, 7–14 (2009).

75. Hoffman, J. D. Anelastic and dielectric effects in polymeric solids, N. G. McCrum, B. E. Read, and G. Williams, Wiley, New York, 1967. pp. 617. $25.00. *J. Appl. Polym. Sci.* **13**, 397–397 (1969).

76. Mangion, M. B. M. & Johari, G. P. Relaxations in thermosets. VI. Effects of crosslinking on sub-Tg relaxations during the curing and aging of epoxide-based thermosets. *J. Polym. Sci. Part B Polym. Phys.* **29**, 437–449 (1991).

77. Nelson, F. C. Vibration Isolation Review: II. Shock Excitation. *Shock Vib.* **3**, 451–459 (1996).

78. Wunderlich, B. *Thermal Analysis of Polymeric Materials*. (Springer-Verlag, 2005). doi:10.1007/b137476.

79. Royall, P. G. *et al.* The development of DMA for the detection of amorphous content in pharmaceutical powdered materials. *Int. J. Pharm.* **301**, 181–191 (2005).

80. Ehrenstein, G. W., Riedel, G. & Trawiel, P. *Thermal analysis of plastics: theory and practice*. (Hanser ; Hanser Gardner Publications [distributor, 2004).

81. Dynamic Mechanical Analysis-Method, Technique, Applications.

82. Maccaferri, E. *et al.* Rubbery nanofibers by co-electrospinning of almost immiscible NBR and PCL blends. *Mater. Des.* **186**, 108210 (2020).

83. NBR. https://polymerdatabase.com/Polymer%20Brands/NBR.html.

84. Burlett, D. J. & Lindt, J. T. Reactive Processing of Rubbers. *Rubber Chem. Technol.* **66**, 411–434 (1993).

85. Poly(ε-caprolactone) (PCL) - Creative Diagnostics. https://www.cd-bioparticles.com/product/poly-caprolactone-pcl-list-216.html.

86. Abedalwafa, M., Wang, F., Wang, L. & Li, C. Biodegradable poly-epsilon-caprolactone (PCL) for tissue engineering applications: A review. *Rev. Adv. Mater. Sci.* **34**, 123–140 (2012).

87. Behera, A. K., Dr. B.B.Barik & Snehal Joshi. POLY-ε-CAPROLACTONE BASED MICROSPHERES AND NANOSPHERES: A REVIEW. *FS J Pharm Res* **1**, (2012).

88. Gupta, B., Geeta & Ray, A. R. Preparation of poly(ε-caprolactone)/poly(ε-caprolactone-co-lactide) (PCL/PLCL) blend filament by melt spinning. *J. Appl. Polym. Sci.* **123**, 1944–1950 (2012).